Bulletin of Volcanology (2025) 87:39
https://doi.org/10.1007/s00445-025-01821-4

RESEARCH ARTICLE

# The influence of moisture on ash strength: implications for understanding volcanic stratigraphy

N. Walding[1,2] · R. Williams[2] · N. Dowey[3] · P. Rowley[4] · M. Thomas[5] · S. Osman[5] · M. Johnson[2] · D. R. Parsons[6]

Received: 4 November 2024 / Accepted: 18 April 2025


## Abstract

Ash layers within extensive pyroclastic density current (PDC) deposits can be important in understanding the evolution of explosive eruptions. If interpreted as ashfall deposits, they may be used to identify hiatus episodes and determine how many pyroclastic density currents were generated during an eruption. However, such layers, which often contain ash aggregates indicating the presence of moisture, may be variably deposited, preserved and eroded, and there has been little study of their characteristics. This paper investigates the geomechanical properties of ash layers through a comparison of field observations and experimental analysis. We present new field evidence of intriguing relationships between ash aggregate layers and overlying ignimbrite facies within the 273 ka Poris ignimbrite of Tenerife. We identify three types of interactions, each displaying distinct erosional and remobilisation behaviours associated with varying moisture conditions. To complement these field observations, we performed direct shear box, ring shear and drop tests under both low (1 wt.%) and high (> 15 wt.%) moisture conditions. We find that fine pyroclastic material increases yield strength with moisture compared to dry conditions. Furthermore, we see shear thickening behaviours in fine ash at high moisture content. These behaviours show how ash layers formed under low and high moisture conditions are more likely to be preserved than dry layers. This may lead to misunderstanding in flow unit interpretation and, therefore, assessments of eruption frequency. Furthermore, dry, loose ash material may promote flow bulking, increasing mobility, runout and flow velocities in PDCs.

**Keywords** Erosion · Entrainment · Remobilisation · Cohesion · Substrate · Sedimentary structures

## Introduction

Pyroclastic density currents (PDCs) are a deadly volcanic hazard that can form during column, lava dome collapse, or lateral blast events (Fisher 1979; Branney and Kokelaar 2002) and pose a significant hazard to communities living around PDC-forming volcanoes (Auker et al. 2013; Lube et al. 2020). PDC activity can be short-lived (seconds to minutes) when associated with lava dome collapse, for example, or can be long-lived and sustained (hours to days) when associated with large-magnitude, caldera-forming eruptions (Fisher 1979; Branney and Kokelaar 2002; Brown et al. 2003; Sulpizio et al. 2014; Lowe and Pittari 2021).

The nature of PDC activity can be determined through visual observation (e.g., Cole et al. 1998) and field study of the resultant pyroclastic material, known as ignimbrite, deposited as these currents move across the landscape (e.g., Fisher 1979). Analysis of ignimbrite stratigraphy has been vital in interpreting the evolution of historic PDC events

Editorial responsibility: M. Edmonds

✉ N. Walding
nwalding@kelpiegeoscience.com

1 Energy and Environment Institute, University of Hull, Cottingham Road, Hull, England HU6 7RX

2 School of Environmental Sciences, University of Hull, Cottingham Road, Hull, England HU6 7RX

3 Geography, Environment and Planning, Sheffield Hallam University, Sheffield, England

4 School of Earth Sciences, University of Bristol, Bristol, England

5 University of Leeds, Leeds, England

6 Loughborough University, Loughborough, England

Published online: 06 May 2025

(e.g., Sigurdsson et al. 1984; Cas and Wright 1987; Druitt et al. 1989; Wilson 1993; Brown and Branney 2004; Lucchi et al. 2018; Dowey and Williams 2022), with stratigraphic data collection informing hazard planning strategies for future eruptions. Flow unit identification (i.e., how many PDCs formed within a single event) may form an essential part of this analysis (e.g., Silva Parejas et al. 2010; Brown and Branney 2013; Douillet et al. 2013; Smith and Kokelaar 2013; Cavazos-Álvarez et al. 2020; Dowey et al. 2024).

A flow unit is best defined as a stratigraphic package of ignimbrite that records the passage of an individual PDC (i.e., one flow unit = one PDC) (Sparks 1976). In a model of progressive aggradation of ignimbrite material (Branney and Kokelaar 2002), flow units are separated by evidence of hiatus where no PDC activity is present in that area at that time. Hiatus layers may be represented by pumice or ash fallout layers, which can represent a change in eruption processes (i.e., during the same eruption), or by evidence of secondary reworking or soil horizons within an ignimbrite sequence which represents a longer time pause or separate eruptions (e.g., Sparks et al. 1973; Sparks and Walker 1977; Wright and Walker 1981; Sigurdsson and Carey 1989; Branney and Kokelaar 1992; Pittari et al. 2006; Brown and Branney 2013; Cavazos-Álvarez & Carrasco-Núñez 2019). Ash fall layers (Fig. 1) can become recorded in an ignimbrite succession during hiatuses in PDC activity either by deposition from the co-ignimbrite plume (i.e., the ash-laden cloud that lofts above a PDC, e.g., Brown and Branney 2004) or from the eruption plume (Brown et al. 2003).

In significant, sustained eruptions, PDC activity can be unsteady through time, displaying phases of waxing and waning due to factors such as changing mass flux at source (Fig. 1) (Pittari et al. 2006; Báez et al. 2020; Charbonnier et al. 2023). Such unsteadiness can cause temporal changes in PDC mobility and run out, both longitudinally away from, and laterally around a volcano (e.g., Williams et al. 2014) and may lead to variable preservation, erosion, or remobilisation of key hiatus indicators such as ash fall layers (e.g., Dowey et al. 2024) (Fig. 2). Such factors can contribute to spatial complexity in the record of hiatus and, therefore, of flow units, leading to contradictory interpretations of eruption history at different locations (Dowey et al. 2024). Understanding the potential for erosion or preservation of these distinct ash layers under various conditions is vital to understanding volcanic sequences, eruption evolution, and hazard identification.

## Changes in variables: flow and deposit

Whether a PDC forms a deposit, erodes the substrate or bypasses an area depends on several factors. Eruption dynamics, such as mass flux and unsteadiness, can vary throughout the lifespan of the current (Bursik and Woods 1996; Pittari et al. 2006; Rowley et al. 2023). Similarly, local environmental conditions play a crucial role in flow behaviours, including surface roughness and topography (Sparks et al. 1997; Brand et al. 2014). These factors influence the fundamental characteristics of the overriding current, such as thickness, particle concentration, pore pressure (Roche et al. 2013) and the resulting conditions at the flow boundary zone at the base of the PDC, which govern the depositional, erosional, or bypassing regime (Brown and Branney 2004; Branney and Kokelaar 2002).

Under depositional or bypassing conditions, an ash layer is more likely to be preserved, whereas erosional conditions may lead to its removal (Brown and Branney 2004). Erosion occurs where erosive forces exceed the resistive forces within the ash material, which include gravity, friction, cohesion, and adhesion (Grabowski et al. 2011). Several factors can influence these forces, such as particle size distribution (Alias et al. 2014), material composition, density, fines content (Jiang et al. 2015; Walding et al. in press), and moisture content (Liu et al. 2022; Walding et al. 2023, in press).

Moisture can be introduced into a PDC from various sources, including pre-eruptive groundwater conditions, surface water interaction and atmospheric humidity (Self and Sparks 1978; Moyer and Swanson 1987; Dartevelle et al. 2002; Cole et al. 2002; Hurwitz et al. 2003; Brown and Branney 2013; Houghton et al. 2015; Pepin et al. 2017; Camuffo 2019; Vecino et al. 2022; Shimizu et al. 2023). Furthermore, post-depositional factors like the extent and type of compaction (e.g., diagenesis) and additional water content (i.e., rainfall) will also contribute to the overall final strength of the ash material (Kim and Sture 2008; Chen et al. 2021a, b; Walding et al. 2023, in press).

## This work and aim

In this work, we investigate the controlling factors governing the strength of fine-grained pyroclastic materials to inform understanding of the fate of ash layer substrates during sustained PDC events. We analyse striking lithostratigraphic relationships observed in moist ash layers on Tenerife where moisture content is inferred by the presence of moisture-induced ash aggregations (Brown et al. 2010, 2012) and hypothesise that the preservation of ash layers depends on their strength, which can be controlled by moisture. The strength behaviours of various pyroclastic ash materials under different moisture conditions, ranging from 1 to 70 wt.%, have been investigated in laboratory tests to better understand these observations. This multidisciplinary work, which brings together volcanic stratigraphers and engineering geologists, aims to quantify the behaviour of volcanic ash in "dry" and "wet" shear environments. These relationships may have significant implications for the preservation or erosion of deposit architecture.

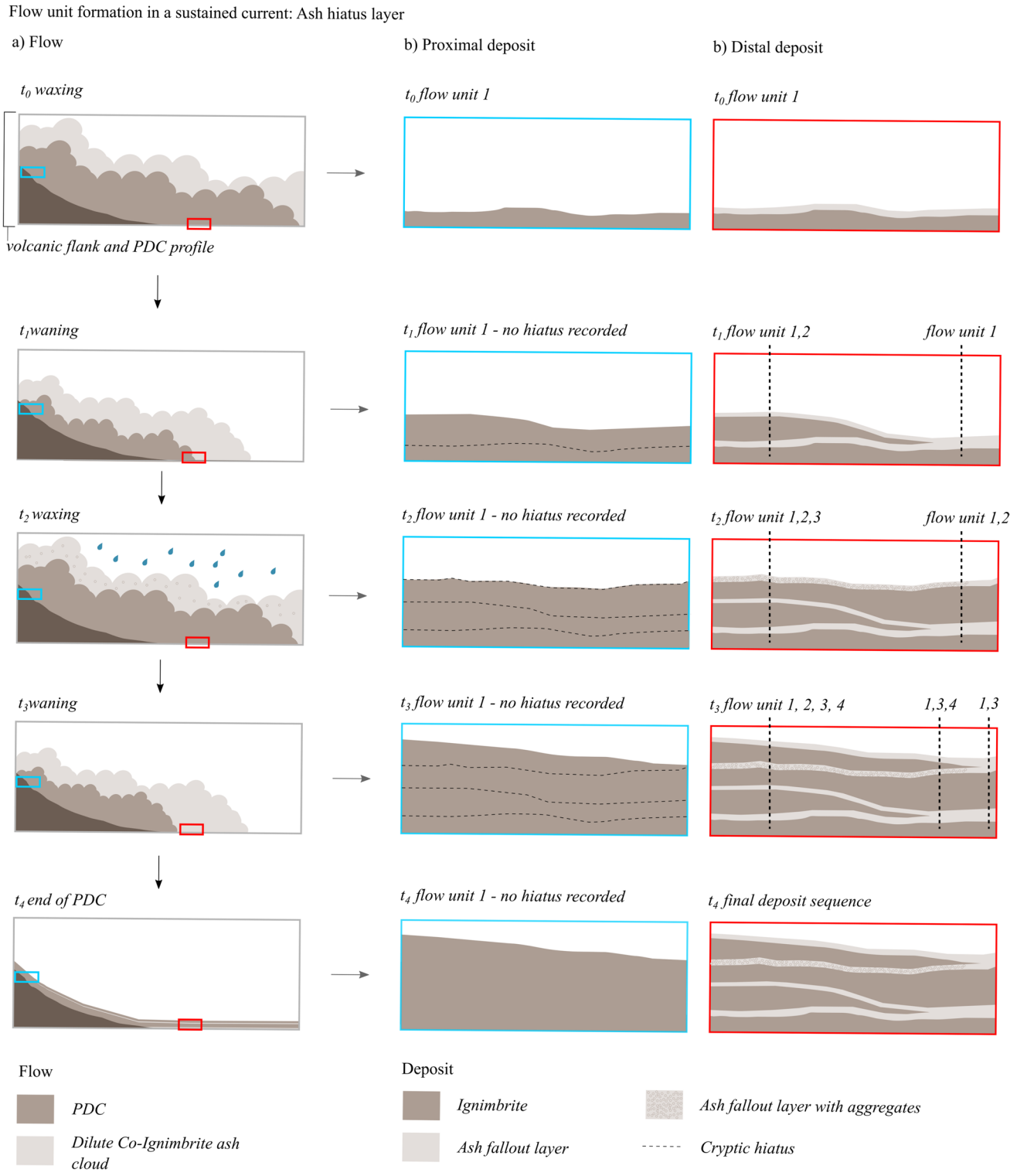


**Fig. 1** Conceptual model depicting how variable deposition of ash fallout layers in proximal and distal locations during unsteady PDC activity can complicate interpretations of flow units and eruption history. As a single PDC undergoes waxing and waning through time and, therefore, changes in run out through time (column a, t0–t4), co-ignimbrite ash is deposited during episodes of local hiatus. Distally (column c), the final deposit may appear to have multiple 'flow units' (dashed line), but only one unsteady PDC was active throughout. Proximally (column b), no evidence of hiatus or 'flow-units' are evident (model based on field correlations presented in Dowey et al. 2024)

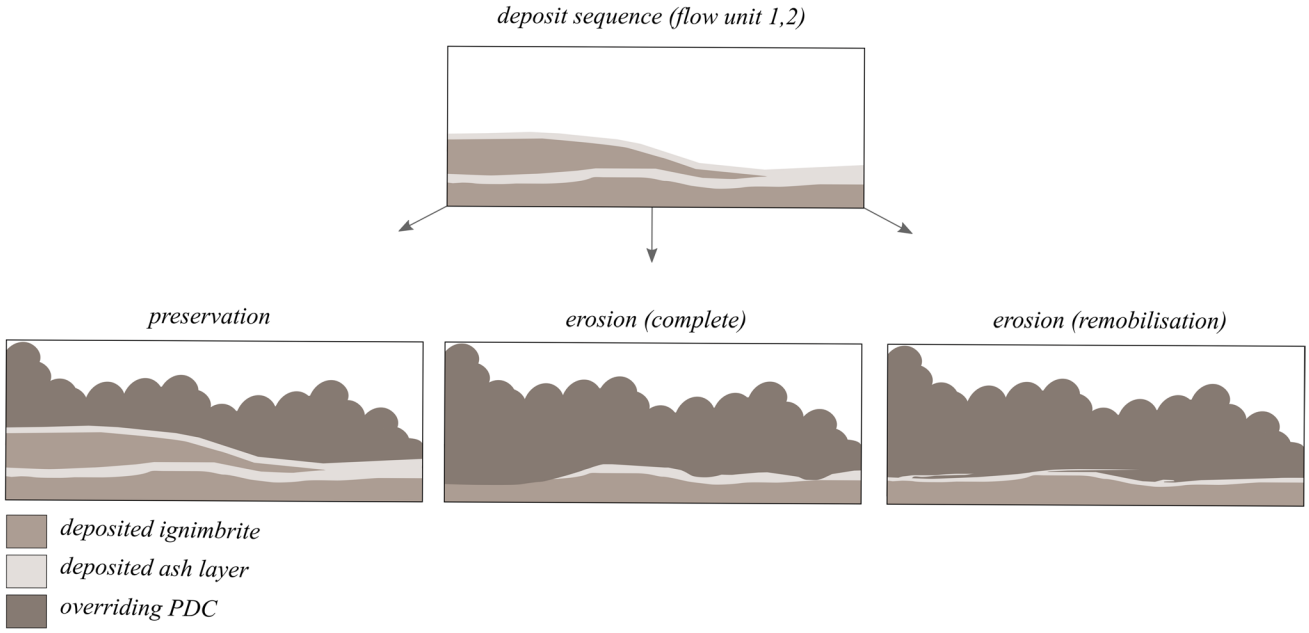


**Fig. 2** Illustration to show how ash layers recording hiatus in an ignimbrite succession may be (**a** preserved, (**b**) eroded, or (**c**) remobilised by subsequent PDC activity, either due to waxing of a sustained unsteady current or by renewed activity following a complete cessation in PDC activity

## Terminology, materials and methods

### Fieldwork terminology

Volcanic ash (pyroclastic material with a particle diameter of < 2 mm, Cas, and Wright 1987) is a fine granular material, and the finest fractions (< 0.064 mm) can be considered a powder. Grainsize controls a variety of changes in the mechanics of how these materials behave, and for this work the more cohesive behaviour of fine powder materials is particularly relevant (Geldart 1973).

Ash aggregates are clusters of volcanic ash particles formed via contact or interstitial forces. They can form due to electrostatic interaction and are found to be prevalent in moisture-influenced conditions (i.e., forming in the presence of rain or high-moisture environments) (Reimer 1983; Gilbert and Lane 1994; Schumacher and Schmincke 1995; Brown et al. 2012; Telling et al. 2013; Diaz-Vecino et al. 2023). Ash aggregates have a higher terminal fall velocity than "dry" ash fallout, due to them being greater in size. They can be found in the ash fall deposits of co-ignimbrite clouds or from plume fallout that records hiatus between distinct episodes of PDC activity (Sparks et al. 1973; Sigurdsson and Carey 1989; Brown and Branney 2004; Pittari et al. 2006; Brown et al. 2010; Dowey et al. 2024).

In this study, we use the term "ash pellet" (AP1 in Brown et al. 2012 scheme) to refer to unstructured ash aggregates that are clast supported and "accretionary lapilli" (AP2 in Brown et al. 2012 scheme) to refer to structured, whole and fragmented ash aggregates that are matrix supported (Supplementary Material A). Both accretionary lapilli and ash pellets can also be formed in central eruption plumes, as well as co-ignimbrite clouds (Brown et al. 2012). On Tenerife, layers of unstructured ash pellets are interpreted to form within moist co-ignimbrite clouds, where ash begins to agglomerate as moisture condenses (Brown et al. 2010). Structured accretionary lapilli with multiple concentric layers have been interpreted to record vertical movement in a PDC system. For example, as accretionary lapilli are lofted and cycled in the thermally stratified area of a PDC, repeating layers of cohesive ash are accreted before lapilli return to relatively drier and hotter zones of the current (Brown et al. 2010). In the context of this work, ash pellets are moist on deposition, and accretionary lapilli are dry and brittle (as evidenced by fragmentation in some cases, Brown et al. 2010).

### Fieldwork stratigraphy and lithofacies

Sedimentological analysis (logging, detailed imaging and sampling) of flow-unit ash layer marker beds and their contacts with overriding deposits was carried out in the Bandas del Sur region of Tenerife (March 2023). Lithostratigraphic features and physical relationships of selected ash layers of the 273 Ka Poris eruption, Tenerife, are reported. The outcrops are located in the Poris Quarry [GR: 2,810,696, 01627001] and Montana Magua [GR: 2,811,244, 01626702] (Figs. 3a.ii, 4a.iii, 5a.ii and 6a.ii). The stratigraphy in these

locations has been worked on extensively by others (Edgar et al. 2002, 2007; Brown et al. 2003; Brown and Branney 2004; 2013). The ash pellet layers investigated here are very-fine- to fine-grained, buff-coloured ash and have been previously interpreted to record local hiatus in PDC activity (Brown and Branney 2004, 2013). Where accretionary lapilli are present, this represents the lofting of pellets in the body of the PDC prior to deposition (Brown and Branney 2004). Lithofacies analysis is based on the approach and descriptions of Branney and Kokelaar (2002), see Supplementary Material B.

## Experimental materials

Through direct shear, ring shear and drop test geomechanical experiments, the properties of a range of fine pyroclastic material at dry, low (1 wt.%) and high (> 15 wt.%) moisture content were explored.

### Material selection

The pyroclastic material studied in the field in Tenerife is lithified and could not be utilised as a loose granular material in laboratory work. Our experiments instead used a suite of fine pyroclastic-ash material from a range of volcanoes (Table 1). Materials < 2 mm were used due to the size restrictions imposed by the shear equipment. The materials were chosen purposefully to span a range of particle sizes, sorting, particle ranges, fines content, composition, and shape characteristics to explore the effect of these variables on moisture and shearing behaviours (Table 2). The materials chosen have been previously described by Walding et al. (2023 and in press). Cornstarch (5–340 µm) was also used as a comparative non-Newtonian synthetic material.

### Material characteristics

Particle size analysis using a CAMSIZER X2 (University of Bristol) was completed to establish the shape and size characteristics of the dry material, with a maximum resolution of 0.8 µm per pixel. Particle size characteristics were measured before and after shear experiments to document physical changes, such as particle crushing.

Sphericity (SPHT) was calculated using Eq. 1, where $P$ is the measured circumference of the particle, and $A_p$ is the area covered by particle projection (see Table 2). An ideal sphere would record SPHT as a value of 1 (Liu et al. 2015).

$$\mathrm{SPHT} = \frac{4\pi A_P}{P^2} \tag{1}$$

Symmetry, which describes the even distribution of the particle around the centre line, was calculated using Eq. 2, where r1 and r2 are minimum and maximum particle radii (Buckland et al. 2021). Symmetrical particles will have a symmetry value of 1, and asymmetrical particles < 1.

$$\frac{1}{2}\left[1 + \min\left(\frac{r_1}{r_2}\right)\right] \tag{2}$$

The particle size data were processed using GRADISTAT (Blott and Pye 2001) to derive particle characteristics using the moments methods (Inman 1952) to calculate logarithmic and geometric mean (($\bar{x}$) ∅), median (∅), range (µm), sorting index ((σ) ∅), sorting ($\sigma \boldsymbol{G}$), skewness (($\boldsymbol{Sk}$) ∅), kurtosis (($\boldsymbol{K}$) ∅), and the geometric mean (µm). Following the approach outlined in Breard et al. (2019), we calculated the $D_{32}$ (mm) and fines content (< 63 µm, %) of the material. $D_{32}$ values, also known as the surface-weighted mean diameter can characterise material fluidisation behaviour (Breard et al. 2019).

$$D_{32}(\mathrm{mm}) = 2 - \left[\mu_{\mathrm{PSD}}(\Phi) + \frac{ln^2}{2}{\sigma_{\mathrm{PSD}}}^2(\Phi)\right] \tag{3}$$

where $\mu_{\mathrm{PSD}}$ and $\sigma_{\mathrm{PSD}}$ are the mean and standard deviation (Eq. 3, Breard et al. in Φ units, 2019).

## Experimental methods

We describe material properties using peak and yield stress, bulk and shear modulus (Sheng et al. 2011; Donaldson et al. 2013; Keaton 2018). Yield stress describes the point at which a material transitions from elastic to plastic behaviour. Elastic deformation describes reversible stretching or compression, where materials with higher elastic moduli are more resistant to deformation. Plastic deformation is irreversible, and the material will continue to deform until it fails at peak stress (i.e., the maximum stress before failure). Therefore, the yield stress measures a material's ability to withstand deformation without failing and, therefore, how less or more likely the material is to move. Similarly, bulk modulus describes the resistance of a material to changes in volume from hydrostatic stress (Donaldson et al. 2013), and shear modulus describes the resistance of a material to shear deformation (Keaton 2018).

We investigated variation in yield strength, bulk and shear modulus using direct and ring shear apparatus at low (1 wt.%) and high moisture (> 15 wt.%) contents (Supplementary Material C). Variations were then explored using the bulk modulus of material at high moisture, with drop test experiments to explore further shear thickening (i.e., non-Newtonian) or shear thinning (i.e., Newtonian) behaviours (Supplementary Material C).

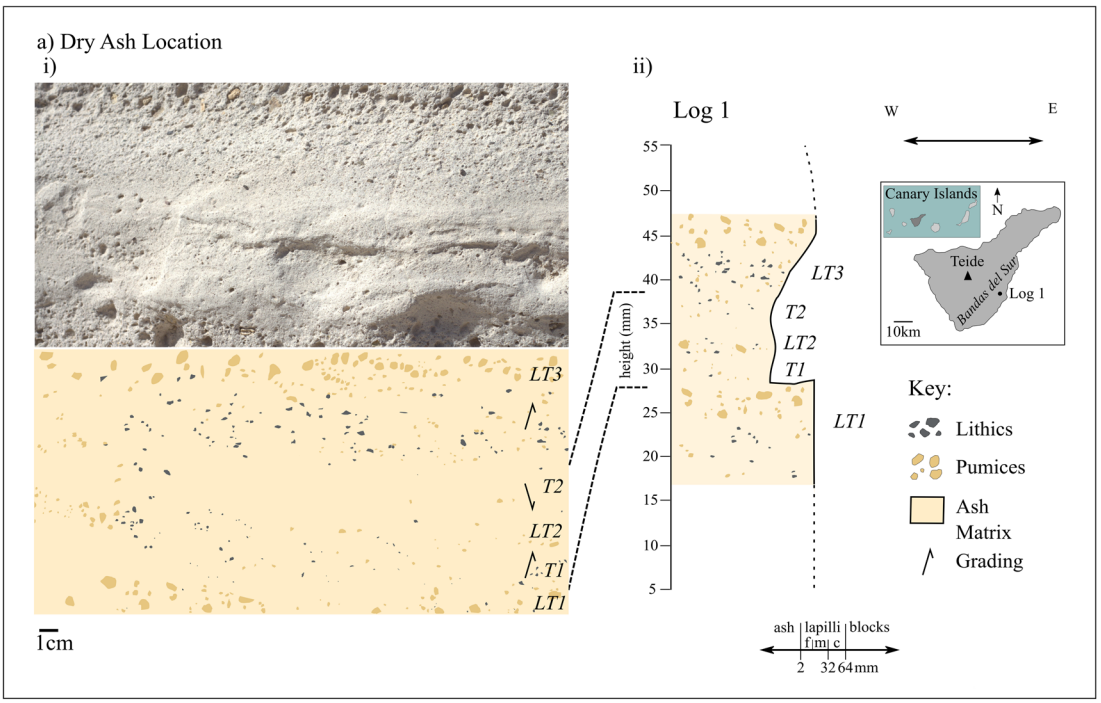
a) Dry Ash Location
i)
ii)
Log 1
W
E
LT3
T2
LT2
T1
LT1
height (mm)
55
50
45
40
35
30
25
20
15
10
5
Canary Islands
N
Teide
Bandas del Sur
Log 1
10km
Key:
Lithics
Pumices
Ash Matrix
Grading
1cm
ash
lapilli
blocks
f
m
c
2
32
64mm

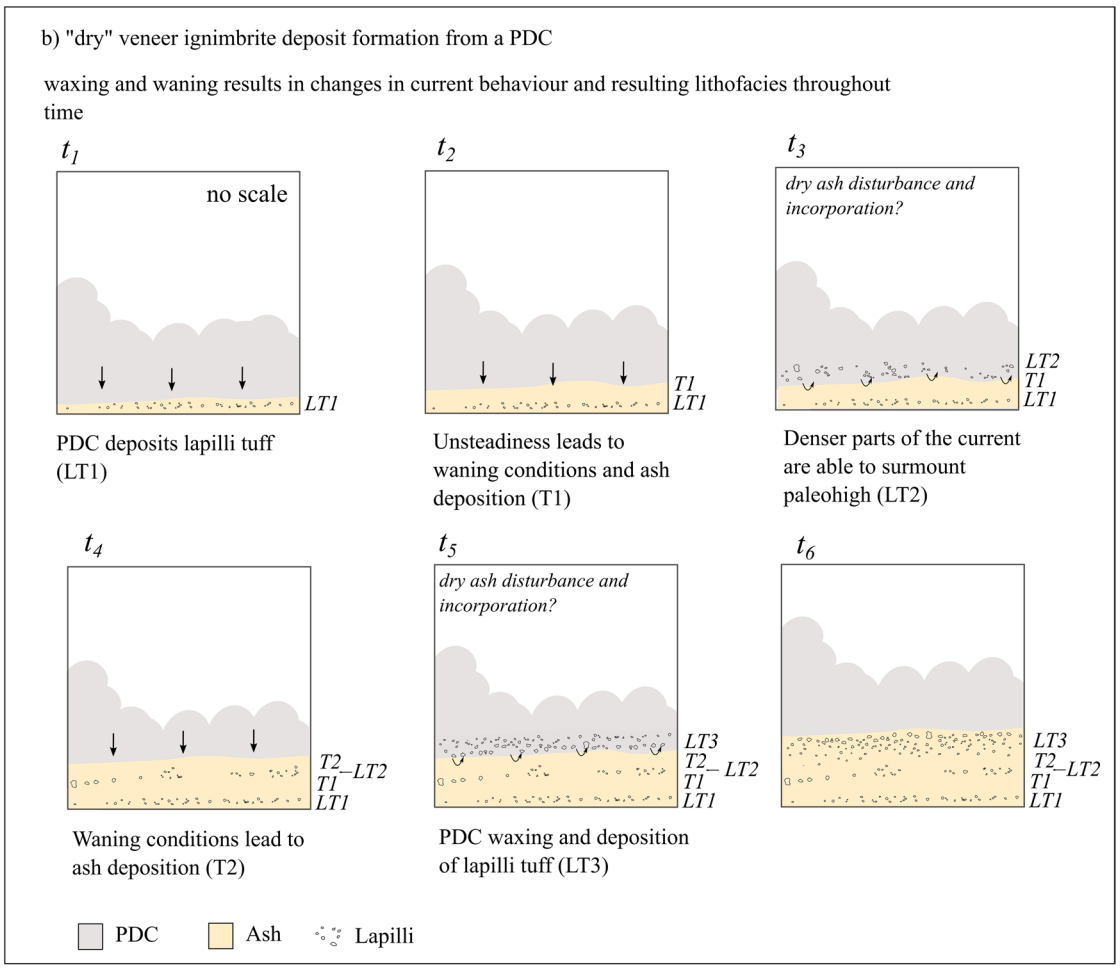
b) "dry" veneer ignimbrite deposit formation from a PDC
waxing and waning results in changes in current behaviour and resulting lithofacies throughout time
$t_1$
no scale
LT1
PDC deposits lapilli tuff (LT1)
$t_2$
T1
LT1
Unsteadiness leads to waning conditions and ash deposition (T1)
$t_3$
dry ash disturbance and incorporation?
LT2
T1
LT1
Denser parts of the current are able to surmount paleohigh (LT2)
$t_4$
T2–LT2
T1
LT1
Waning conditions lead to ash deposition (T2)
$t_5$
dry ash disturbance and incorporation?
LT3
T2– LT2
T1
LT1
PDC waxing and deposition of lapilli tuff (LT3)
$t_6$
LT3
T2–LT2
T1
LT1
PDC
Ash
Lapilli

◂**Fig. 3** **a.i** Ash-rich lapilli-tuff (LT1, LT2 and LT3) in contact with tuff (T1 and T2) within the Cueva Honda member of the Poris Formation at Montaña Magua. **a.ii** Location map, log at GR: 2,811,282, 01626695. See lithofacies terminology in Supplementary Material B. **b** Interpretation of the formation of deposits shown in Log 1 through time (t) (see text for explanation)

### Direct shear

Direct shear tests (Supplementary Material C, e.g., Niroumand 2017) were performed to determine the shear strength of pyroclastic materials with the addition of moisture. These were completed using the direct shear apparatus (Faculty of Engineering, University of Bristol). Three experiments were undertaken on 200 g of various materials (Tung 1, Tung 4, Tung 5 and Colima) at 0, 0.25, 0.50, 1 and 5 wt.% moisture. Samples were dried at 80 °C for 24 h before the experiments to ensure the removal of adsorbed moisture. Agglomerations were broken up by sieving before the addition of water. On addition of moisture, the samples were thoroughly mixed to ensure an even moisture distribution.

For each experiment, the material was loaded into the shear cell (60 × 60 mm) and consolidated for 20 min prior to shearing. The consolidation and shear tests were completed under a normal stress of 1, 14 and 27 kPa. These normal stress values were chosen to encompass a range of loads and to ensure behaviours were seen in a dry and wet (by adding moisture) state without generating pore pressure. The shear test was then completed at a 1 mm/min rate until peak shear was reached or the shear box length limited completion. Experiments were also completed at 0.5 mm/min to ensure we were not seeing significant influence from pore pressure. The results from the 0.5 mm/min tests are reported in Supplementary Material D and show similar results to that of the 1 mm/min tests. Therefore, we can conclude that pore-pressure is not being generated by higher shear rates, so is not affecting our results.

### Ring shear

A suite of fine pyroclastic material (< 1 mm) with varying moisture contents was tested in the Imperial College Ring Shear apparatus (Supplementary Material C, Bishop et al. 1971) at the University of Leeds, in order to inform interpretations of PDC behaviours made from stratigraphic relationships in Tenerife. Brown Tuff, Atitlan 2 and Taupo 1 (Table 2) samples were used for ring shear testing, to represent fine ash materials with high fines content. The samples were prepared as in the direct shear box tests.

The ring shear comprises two split confining rings with an outer diameter of 152.4 mm and an inner of 101.6 mm (Supplementary Material C). The depth of the sample area is 19 mm. Around 150–200 g of samples were used to run each experiment; variations in sample weight were due to changes in the density of the material and the required amount to fill the chamber. Each material was weighed before and after loading the shear chamber. The samples were sieved and sheared initially when dry (0 wt.% moisture). The initial set of experiments records the consolidation of the sample under a varying normal weight load. The second set of experiments records the shear behaviour of the samples. We then introduced water (0.5 and 1 wt.%) into the sample and repeated the experiment. Due to time constraints, higher moisture contents were not tested.

The ring shear tests were performed at constant normal stresses of 5, 10 and 20 kPa for each water addition. For each experiment, consolidation and shear measurements were recorded every 1 s for the first hour, then every minute for an hour and finally every half-hour for the remainder of the experiment. Shearing was completed at a shear rate of 1.0 deg/min. The relative horizontal shear and vertical displacement were recorded, with the latter being measured through compaction or dilation of the material. It should be noted that the right proving ring sensor had fluctuating background noise that resulted in noisy results. This was reduced by using a moving average of the results.

The Mohr–Coulomb failure criterion describes the failure of materials where peak shear stress values are determined by cohesion and internal friction angle (Massoudi and Mehrabadi 2001). Using the Mohr–Coulomb failure criterion on the normal stress and peak stress values, we determined friction angle (the ability of a material to withstand shear stress, therefore, higher resistance to erosion), cohesion and dilation (i.e., shear thickening) and compaction (i.e., shear thinning).

### Drop test

The drop test (Supplementary Material C, Crawford et al. 2013) was conducted on the Atitlan 1, Colima, Taupo 1, Taupo 2 and Tung 6 pyroclastic materials at varying states of high-water addition to explore the effects of shear thickening and thinning behaviours. Cornstarch and water (also named Oobleck), saturated at 75 wt.% moisture was used as a comparison sample to show explicit shear thickening behaviours.

A steel ball (20 mm diameter, 7910 kg/m$^3$) was dropped from a height of 270 mm onto loose material saturated at 0, 15, 25, 30, 40, 50, 60, 70 and 90 wt.% in a clear box (60 × 60 × 60 mm). Each experiment was completed three times. Video footage (700 fps), using a high-speed camera (Phantom VEO 440), recorded the steel ball hitting the sample. The footage was then analysed using ImageJ (Schindelin et al. 2012) to observe the nature of the interaction of the falling ball with the material deposit (i.e., the ball sinking through the deposit or the ball bouncing off the deposit). After each experiment, the ball penetration depth (i.e., how

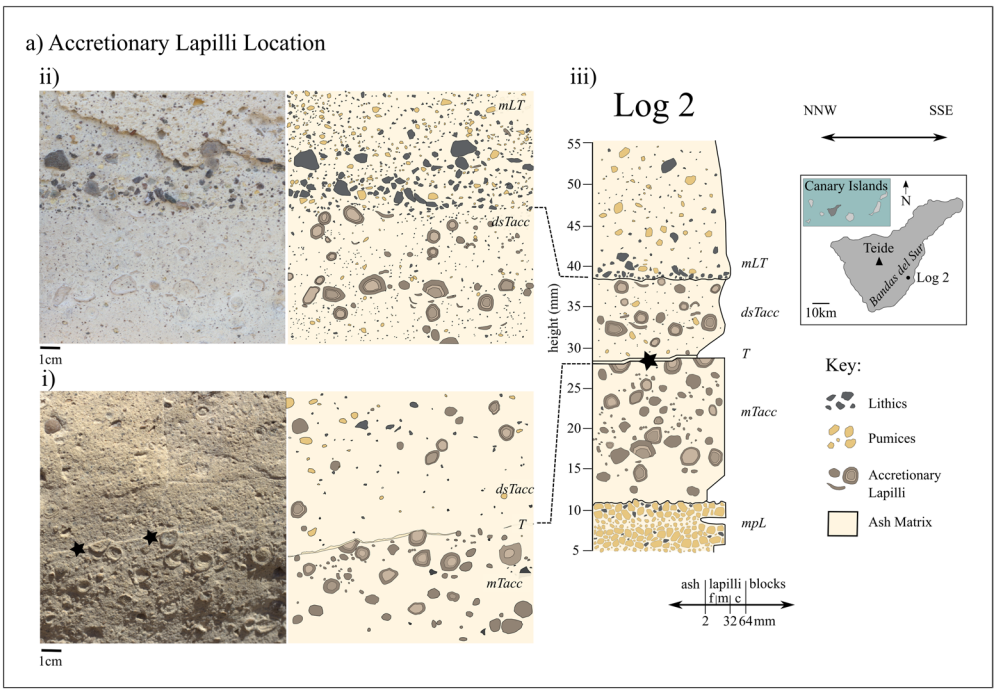
a) Accretionary Lapilli Location
ii)
mLT
dsTacc
1cm
i)
dsTacc
T
mTacc
1cm
iii)
Log 2
NNW
SSE
Canary Islands
N
Teide
Bandas del Sur
Log 2
10km
height (mm)
55
50
45
40
35
30
25
20
15
10
5
mLT
dsTacc
T
mTacc
mpL
ash | lapilli | blocks
f | m | c
2 32 64mm
Key:
Lithics
Pumices
Accretionary Lapilli
Ash Matrix

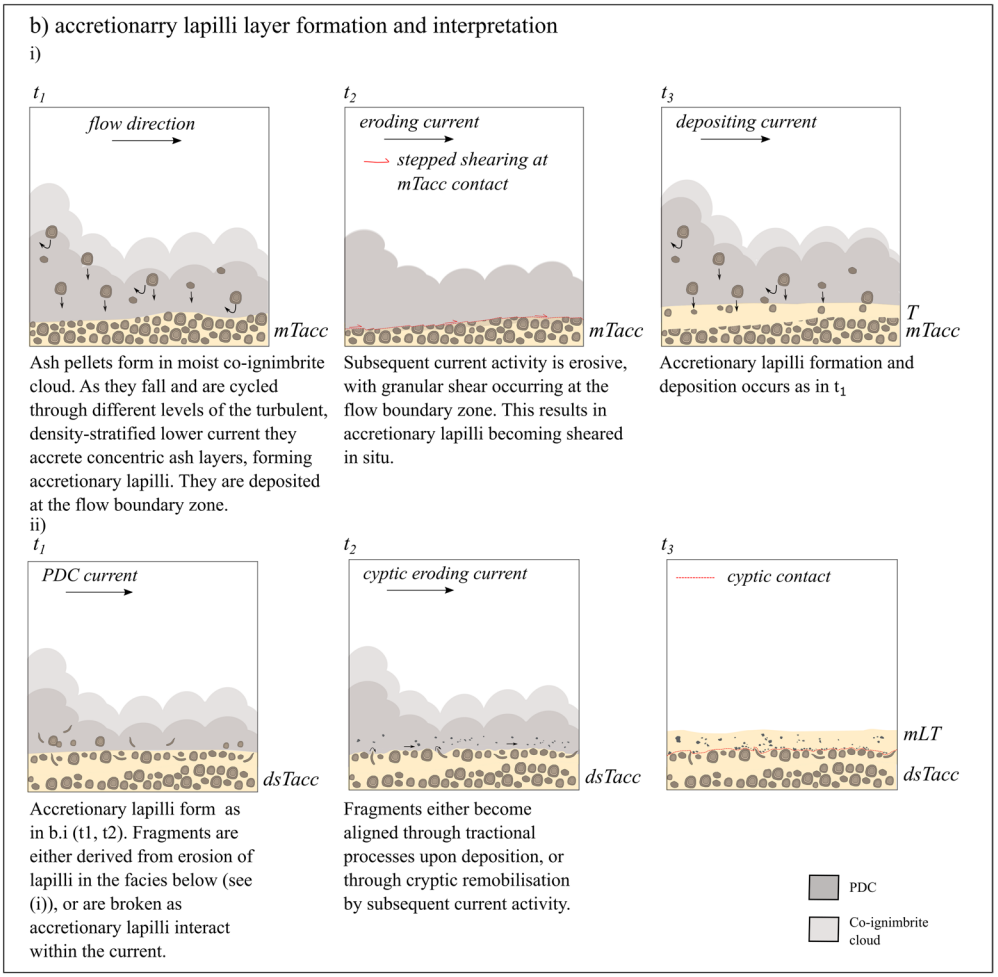
b) accretionarry lapilli layer formation and interpretation
i)
t1
flow direction
mTacc
Ash pellets form in moist co-ignimbrite cloud. As they fall and are cycled through different levels of the turbulent, density-stratified lower current they accrete concentric ash layers, forming accretionary lapilli. They are deposited at the flow boundary zone.
t2
eroding current
stepped shearing at mTacc contact
mTacc
Subsequent current activity is erosive, with granular shear occurring at the flow boundary zone. This results in accretionary lapilli becoming sheared in situ.
t3
depositing current
T
mTacc
Accretionary lapilli formation and deposition occurs as in t1
ii)
t1
PDC current
dsTacc
Accretionary lapilli form as in b.i (t1, t2). Fragments are either derived from erosion of lapilli in the facies below (see (i)), or are broken as accretionary lapilli interact within the current.
t2
cyptic eroding current
dsTacc
Fragments either become aligned through tractional processes upon deposition, or through cryptic remobilisation by subsequent current activity.
t3
cyptic contact
mLT
dsTacc
PDC
Co-ignimbrite cloud

◂**Fig. 4** **a.i** Accretionary lapilli layer (mTacc) in contact with overlying thin tuff (T) layer, observed in the Magua Member of the Poris Formation at Montaña Magua [GR: 2,811,244, 01626702]. Accretionary lapilli are sheared at the contact (star). **a.ii** Diffuse stratified accretionary lapilli unit (dsTacc) in contact with overlying lapilli-tuff layer (mLT). Accretionary lapilli are fragmented at the contact. **a. iii** Location map, log at GR: 2,811,244, 01626702. See lithofacies terminology in Supplementary Material B. **b** Interpretation of formation of **i** the lower contact (4a.i) showing granular shear occurring at the flow boundary zone in log 2, and **ii** the more cryptic upper contact shown in log 2 (see text for full explanation)

far the ball made it through the deposit) was measured to gain insight into the material's resistance under varying moisture.

## Variations in ash layer strength on Tenerife

### "Dry" ash layer contact

At the Montaña Magua location on Tenerife (Fig. 3a), two contacts between ash (T) and lapilli-tuff (LT) occur within the Cueva Honda member (< 0.90 m thick, distributed from La Caleta to Montaña Magua) of the Poris Formation (flow unit 3, member 7, Brown and Branney 2004, 2013).

At this location, ash layers (T1 and T2) occur between lapilli-tuff lithofacies (LT1, LT2, LT3). The contact between lapilli tuff (LT1) and tuff (T1) is typically clear and well-defined, whilst the upper contact between the tuff (T2) and lapilli tuff (LT3) is more graduated and diffuse, occasionally displaying grading. The ash layers (T1 and T2) are well sorted and normally graded into lapilli tuff. The second lapilli tuff layer (LT2, sandwiched between T1 and T2) contains pumice, lithics, and some eroded remnants of sub-rounded pumice clasts and shows no sign of ash aggregates (Fig. 3a).

#### Interpretation

This ash layer is interpreted to be an ignimbrite veneer, which is a thin ignimbrite layer deposited by dilute parts of a PDC that can surmount topographic palaeohighs (Branney and Kokelaar 2002; Brown and Branney 2004; flow unit 3, member 6, Brown and Branney 2013). The lack of ash aggregates indicates formation in low-humidity or high-temperature environments with little external influence of moisture (such as precipitation or steam).

Transitions from lapilli tuff to ash, and then back to lapilli tuff, reflect unsteadiness in PDC dynamics (and therefore changes in flow boundary zone conditions) through time (t1–t5, Fig. 3b). Waxing or waning energy in the system may have led to the varying ability of denser parts of the current to surmount topography. The diffuse and graded nature of the contact, together with evidence that these ash layers were dry and likely loose on deposition, makes it seem likely that the ash layers were disturbed, remobilised and potentially incorporated into subsequent lapilli tuff layers as they were deposited (t3 and t5).

### Sheared accretionary lapilli ash layer contact

Two subtle, cryptic contacts were identified at Montaña Magua, at different stratigraphic levels within the Magua Member (< 15 m thick, flow unit 3, Member 6 in Brown and Branney 2004) of the Poris Formation (Fig. 4). At this location, the Magua Member consists of a fine-grained tuff containing scattered accretionary lapilli ranging from 3 to 30 mm in size (Brown and Branney 2004; Brown et al. 2003; Brown et al. 2010).

The first contact occurs between an accretionary lapilli-rich ash layer (mTacc in Fig. 4a.i) and a < 3 mm thick tuff layer above (T), which is then overlain by a diffusely stratified accretionary lapilli layer (dsTacc). In the lower aggregate-rich layer (mTacc), accretionary lapilli are mostly intact and unfragmented; however at the contact with the tuff, which is irregular with an undulating or stepped appearance (Fig. 4a. i), accretionary lapilli are sheared in situ.

The overlying diffusely stratified accretionary lapilli facies (dsTacc) contains vertical transitions from increased to decreased accretionary lapilli concentrations. The second distinct contact, between this facies and massive lapilli tuff (mLT) above, is marked by a difference in lithic content (Fig. 4a.ii). In the diffusely stratified facies (dsTacc), accretionary lapilli are mostly intact, although occasional angular accretionary lapilli fragments (< 20 mm) appear aligned with flow direction. In some areas, ash at the base of the massive lapilli facies (mLT) appears to be draped over whole accretionary lapilli, with no evidence of shear or erosion.

#### Interpretation

The lower contact between the accretionary lapilli (mTacc) and ash layer (T) is sharp and stepped and is interpreted to have formed through abrasion during low-impact granular shear in the lower regions of the current (Fig. 4b.i, Branney and Kokelaar 2002; Brown et al. 2010). This observation is significant because layers rich in accretionary lapilli are thought to form during fluctuating current intensity (waxing and waning), perhaps making them unlikely to be fully cemented during the brief deposition period (Brown et al. 2010). However, in this example, the resistance of the accretionary lapilli to plucking from the substrate, the lack of disaggregation, and the planar erosion (shearing) through some of the lapilli suggest that both the accretionary lapilli (mTacc) and the ash (T) layer in which they were deposited had considerable strength. This strength during deposition

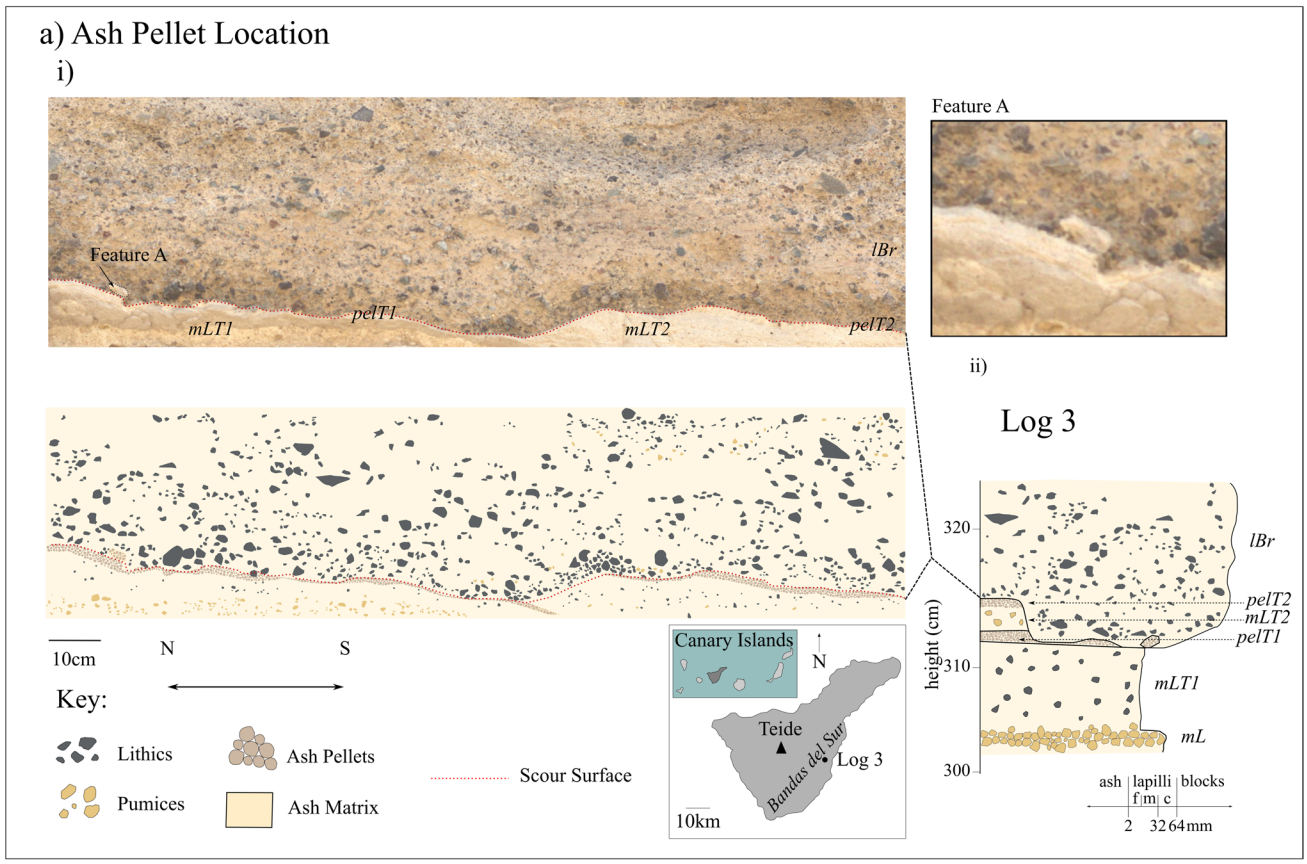


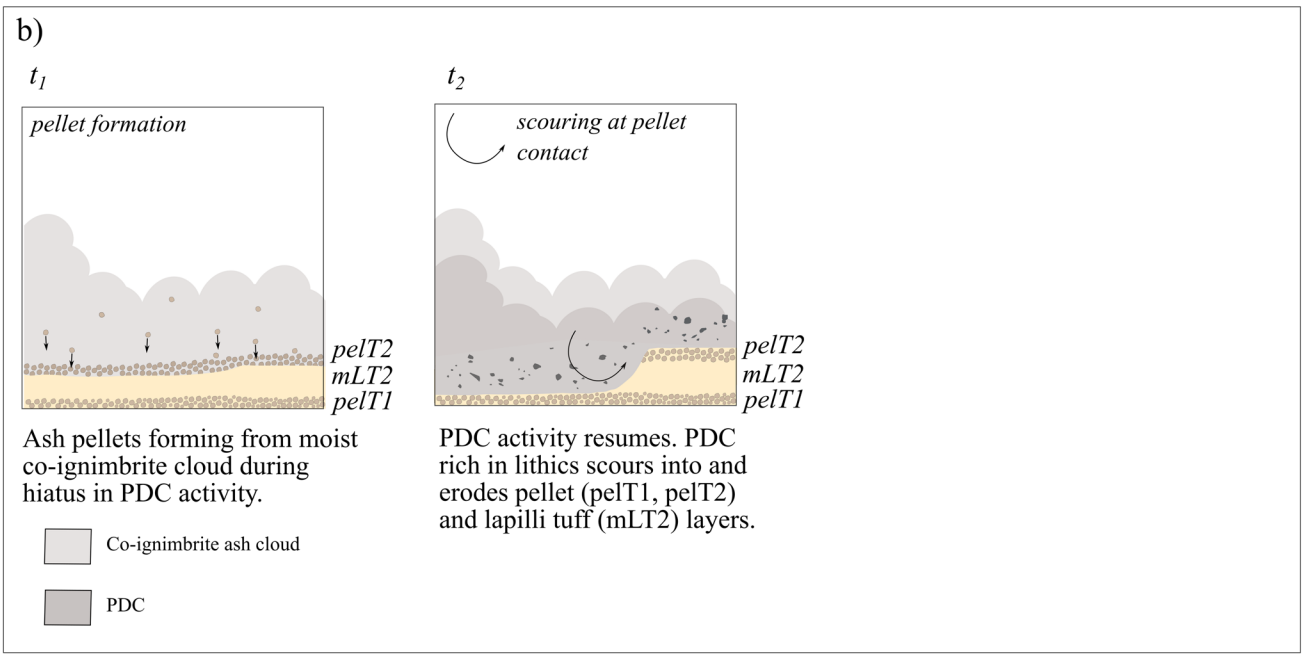


**Fig. 5** **a** Ash pellet (pelT1 and 2) layers documenting an episode of PDC hiatus in this area. The ash pellet layers (pelT1 and 2) of the Jurado Member of the Poris ignimbrite (Brown and Branney 2004) are in erosive scouring contact with the lithic breccia (lBr) facies above (red dashed line). **i** Ash pellet contact (pelT1) is overlain by lapilli tuff (mLT2). Feature A indicates remobilisation. The second ash pellet layer (pelT2) is overlain (in erosive contact) by the lithic breccia unit (lBr). **ii** Location map, log at GR: 2,810,693, 01627006. See lithofacies terminology in Supplementary Material B. Flow direction is north to south. **b** Interpretation panels showing (t1) the formation of the ash pellet layers and (t2) erosion of ash pellets and lapilli tuff by subsequent lithic-rich PDC activity (see interpretation text for full explanation)

has previously been attributed to the precipitation of salt or other minerals, which may have caused cementation of the ash (Zeolite, Brown and Branney 2004; Mueller et al. 2017), or from "baking" of the lapilli when moving through high-temperature areas of the PDC during lofting (Brown and Branney. 2004). A lack of fragmentation within the accretionary lapilli layer (mTacc) beneath the contact zone suggests that when the facies was deposited, the current was sufficiently dilute as to not induce breakage (Mueller et al. 2017).

The upper contact between the diffuse stratified accretionary lapilli (dsTacc) and lapilli tuff layer (mLT) contains fragmented accretionary lapilli with some directional fabric to them. This indicates that the current conditions were concentrated and sufficiently energetic to enable interactions and breakage (Mueller et al. 2017). This may be due to tractional processes during the deposition of the fragments, or through cryptic remobilisation by subsequent current activity. In addition to these fragmented lapilli, intact, non-sheared accretionary lapilli are also observed, protruding from the ash layer without signs of erosion from the overriding current (Fig. 4.ii).

## "Wet" ash pellet layer contact

At the Poris Quarry, distinct layers of pellets are present that are associated with the Jurado Member of the Poris Formation (Brown and Branney 2004) and a sequence containing ash pellet-rich tuff (pelT) is observed (Fig. 5a). A massive lapilli tuff facies (mLT1), characterised by a poorly sorted lithic and pumice lapilli within an ash matrix, occurs in contact with a pellet-rich ash layer (pelT1). Another lapilli tuff layer (mLT2) occurs above this, in sharp contact with the pellet layer below with little evidence of erosion, and is overlain by a second ash pellet layer (pelT2). All of these units are discontinuously preserved due to erosive contact with an overlying lithic-rich facies (lBr). This lithic breccia facies is observed cutting down into the sequence, with an undulous, scouring contact at its base (indicated by dashed red line in Fig. 5a.i), and in some places both pellet layers are completely absent. In one location (Feature A, Fig. 5a.i), a clump of the first pellet layer is seen to be detached and rotated from its original stratigraphic position within the lithic breccia facies.

### Interpretation

The ash pellet layers (pelT1 and pelT2) at Poris Quarry represent direct fallout from a moist co-ignimbrite plume (Fig. 5b) (Brown and Branney 2004, 2013; Brown et al. 2010), marking a hiatus in PDC activity. Unlike accretionary lapilli, ash pellets do not loft within the turbulent PDC, so their deposition signifies a temporary break in PDC activity in this area. Furthermore, the pellets identified in this area are considered moist on deposition due to the lack of internal laminations and evidence of amalgamation with surrounding pellets (Brown and Branney 2004).

The lapilli tuff layer (mLT1) indicates PDC activity in the area followed by a hiatus ash pellet layer (pelT1). The second lapilli tuff layer (mLT2) indicates resuming PDC activity but is not seen to erode the underlying ash pellet layer (pelT1) (Fig. 5a.i). This facies is overlain by the second ash pellet layer (pelT2) marking further hiatus. Activity then resumes, and a lithic-rich, erosive current scours into, remobilises (Feature A), and sometimes completely removes, the underlying layers (Fig. 5, pelT1, mLT2, and pelT1). It is possible that, prior to the lithic-rich activity recorded here, other facies were deposited and completely removed from the record due to this erosion. However, lithic-rich facies have been linked to waxing current activity (as a result of events such as incremental caldera collapse) elsewhere in the Poris Formation (Brown et al. 2003; Smith and Kokelaar 2013), and it seems sensible to infer that PDC activity resumed at this location following a period of hiatus due to current waxing, marked by increased lithics.

The nature of the relationship between the lithic breccia facies and the ash layers below is a strong indication that these lithics were responsible for the erosion (as opposed to the erosional surface marking an episode of scour and bypass onto which lithics from subsequent activity were deposited). Feature A (Fig. 5a) is particularly important. It shows the remobilisation of a portion of the pellet layer as a "rip-up clast," indicating a dynamic, shearing depositional environment at the interface between the lithic-rich current and the ash pellet (pelT1) layer. The ash pellet (pelT1) layer must have had an inherent strength to remain intact as a coherent package and to withstand shearing.

## Ash layer remobilisation

A buff-coloured and fine-grained ash layer (T*) occurs in the Poris Quarry [GR: 2,810,696, 01627001]. It is observed between a lapilli tuff facies below (mLT) and a lithic breccia facies above (lBr) (the lithic-rich Tamadaya Member of Brown and Branney 2004).

The ash layer (T*) is high in the sequence (~ 5 m above the ground), so the presence of ash aggregates could not be observed. However, a "*" notation is used here to indicate the high likelihood that this facies contains ash pellets or accretionary lapilli, due to its position at a similar stratigraphic level as other pellet layers in the sequence, and from descriptions in Brown and Branney (2004). The ash layer (~ 10 cm thick, and traced for ~ 2.5 m) is distinctive because it exhibits a zone of unique "peeling" and "lifting" in a hockey-stick shape.

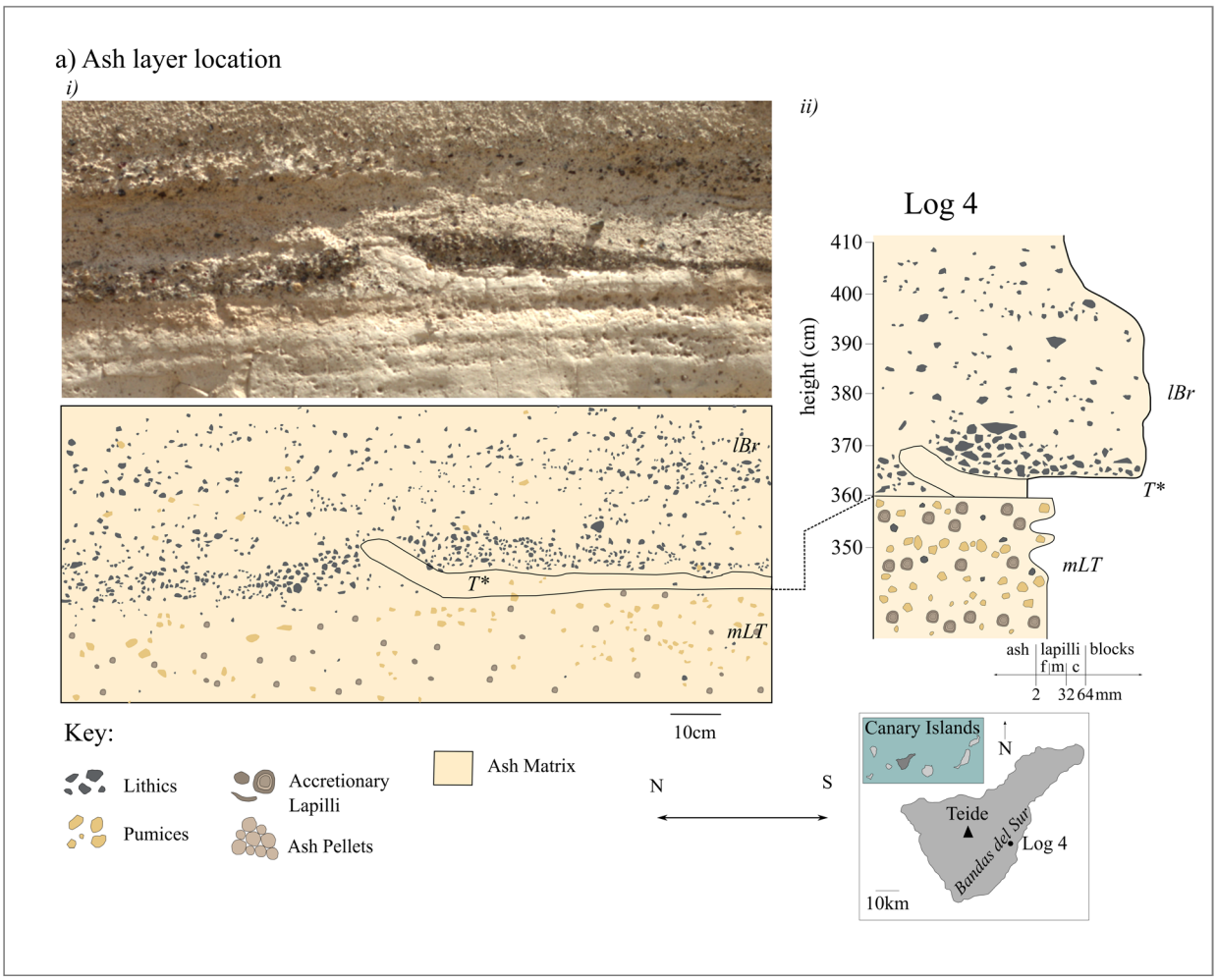
a) Ash layer location
i)
ii)
lBr
T*
mLT
Log 4
height (cm)
410
400
390
380
370
360
350
ash
lapilli
blocks
f
m
c
2
32
64mm
10cm
Key:
Lithics
Pumices
Accretionary Lapilli
Ash Pellets
Ash Matrix
N
S
Canary Islands
Teide
Log 4
Bandas del Sur
10km
b) T* layer remobilisation
$t_1$
$t_2$
$t_3$
shearing at pellet contact
Lithic rich PDC moving over the T* contact.
Tractional shearing at the base of the PDC causes the T* layer to lift.
Continued shearing with deposition.
Co-ignimbrite ash cloud
PDC

◂**Fig. 6** **a.i** Ash layer (T*) in contact with overlying lithic-rich facies (lBr) in the Jurado and Tamadaya Member of the Poris Ignimbrite (Brown and Branney 2004) at the Poris Quarry location. Note the 'peeling up' and lifting of the coherent zone of ash. **ii** Location map, log at GR: 2,810,696, 01627001. See lithofacies terminology in Supplementary Material B. Flow direction is north to south. **b** Interpretation panels showing the formation of this striking feature at the ash layer contact (see text for full explanation)

#### Interpretation

The ash layer (T*) is interpreted to record fallout from a moist co-ignimbrite plume during an episode of hiatus in main current activity (Fig. 6b.i; Brown and Branney 2004), similar to the ash pellet layer described in the "Wet" ash pellet layer contact section (Fig. 5). The 'hockey-stick' structure (Fig. 6a) is interpreted to record remobilisation of coherent sections of the ash pellet layer due to shearing at the base of a subsequent PDC.

Field observations by Brown and Branney (2004) describe the pellet layers as traceable units, though they are often eroded by subsequent PDCs, leading to inconsistent preservation; this locality provides direct evidence of erosional processes in action. The high lithic content of the breccia (lBr) indicates waxing conditions and the influx of lithics at the source, such as that associated with incremental caldera collapse (Brown et al. 2003; Brown and Branney 2004; Smith and Kokelaar 2013). The interaction of this more concentrated, dense current with the underlying ash layer likely represents a significant change in shear and load behaviours at the flow boundary zone. Despite uncertainty in the nature of the aggregate content, this feature indicates the coherence of this ash layer.

### Questions raised by the fieldwork

The field analysis presented here documents ash layers in various contact relationships. One layer, interpreted as 'dry' due to a lack of ash aggregates, shows no evidence of resistance to erosion by subsequent activity. Other ash layers, interpreted to have formed under either high or low moisture conditions by their ash aggregate content, are associated with intriguing shear relationships indicating resistance to erosion.

The preservation, or not, of these layers appears to be linked to their inherent strength, which we hypothesise is influenced by moisture content. This raises the question of how moisture influences the strength and, therefore, behaviour and preservation of an ash substrate during subsequent PDC activity. Improved understanding of this issue has implications for our interpretation of volcanic stratigraphy and hiatus layers, particularly for inferences of the number of PDCs formed during an eruption. In the following section, we investigate how moisture affects ash layer strength and vulnerability to erosion to gain a more comprehensive understanding of the dynamics and preservation of ash layers seen in PDC deposits.

## Experimental results

Shear tests were completed to determine how the strength of material changes in dry (0 wt.%) and moist (> 0 wt.%) conditions. We hypothesise that the presence of moisture-induced ash aggregates may increase the yield strength of the material, thereby affecting its ability to be eroded or remobilised.

### Direct shear box tests

Direct shear experiments were performed on four samples from 0 to 5 wt.% moisture. The peak stress was not reached during the duration of the experiments (Fig. 7). Therefore, we completed the remaining experiments using the ring shear apparatus, employing finer sized material to better reflect the fine ash as seen in Tenerife. The results of the direct shear box are in Supplementary Material E.

### Ring shear tests

The ring shear tests allow us to see the full extent of the shear profile, which was unable to be observed in the direct shear box. The ring shear tests were performed on three samples with 0 and 1 wt.% moisture content.

At 0 wt.% moisture (Fig. 8), Brown Tuff (mean size 3.55 ϕ, 29.35% fines) and Taupo 1 (mean size 2.08 ϕ, 38.90% fines) showed increasing peak shear stress with increasing normal stress (Table 2). The peak shear stress was reached in a 5–20 mm shear distance, although it ran for much longer distances. Atitlan 2 (mean size 3.44 ϕ, 40.57% fines) showed an unexplained decreasing peak stress with increasing normal stress (Table 2, Fig. 8a).

At 1 wt.% moisture, Taupo 1 and Brown Tuff (Fig. 8b, c) again behave as expected, with peak stress increasing with normal stress. Similarly to the 0 wt.% moisture experiments, Atitlan 2 showed an unexplained decreasing peak stress with normal stress (Fig. 8a). The peak shear stress of all 1 wt.% moisture samples was reached in a shear distance of 5–10 mm.

Zones of elastic and plastic deformation separated by a region of yield have been identified (labelled B; Fig. 8). In the elastic zone, material can deform but return, while plastic behaviour occurs when deformation is permanent after exceeding the sample's yield. Our results show that at 0 wt.% moisture, the region of yielding is consistently reached in the first 16 mm of shearing across all normal stresses. The

**Table 1** Experimental material source location, chemical composition, formation mechanisms and the test completed in this work. DS – direct shear, RS – ring shear and DT – drop test. References detail material characteristics, collection and location

| Material | Composition | Formation | References | Test |
|---|---|---|---|---|
| Tung 1, 4, 5, 6 (Tungurahua, Ecuador) | Andesitic | 2006 VEI 3 eruption. Sampled at different localities | Hall et al. 2007; Kelfoun et al. 2009; Douillet et al. 2013; Eychenne et al. 2012 | DS – Tung 1,4 and 5<br>DT – Tung 6 |
| Atitlan 1 (Guatemala) | - | Volcán de San Pedro. Unstudied ignimbrite deposit GR: 14°40′55.24"N, 91°15′29.15"W | Rowley, P. *In comms* (2023) | DT |
| Atitlan 2 (Guatemala) | Andesitic | Los Chocoyos eruption (80.6 ka) of Atitlan Caldera. GR: 14°48′54.74"N, 91°12′27.37"W | Rowley, P. *In comms* (2023) | RS |
| Brown Tuff (Lipari, Italy) | - | La Fossa Caldera, 80–60 ka. GR: 38°28′46.5"N, 14°57′32.2"E | - | RS |
| Taupo 1 (New Zealand) | Rhyolitic | 253 AD eruption. Sampled 17 km from vent | Wilson (1985) | RS, DT |
| Taupo 2 (New Zealand) | Rhyolitic | 232 AD eruption. Sampled 2–8 km from vent | Wilson (1985) | DT |
| Colima (Mexico) | Andesitic | Volcán de Colima, México, 2015. GR: 19°43′92.22"N, −103°61′47.05"W | Johnston, T. *In comms* (2023) | DS, DT |
| Cornstarch (synthetic material comparison) | Cornstarch | - | Walding et al. in press | DT |

average linear displacement required to reach the yield increases with load and decreases with moisture addition.

For the Taupo 1 sample, the application of the Mohr–Coulomb failure shows an internal friction angle of 31° and cohesion value of 0.6 kPa for the dry (0 wt.% moisture) and an internal friction angle of 48° and cohesion value of 1.1 kPa for the 1 wt.% moisture conditions. Brown Tuff results show internal friction angles of 29° and 22° and a cohesion value of 0.56 and 0.42 kPa for 0 and 1 wt.% moisture, respectively. The decrease in values seen for the Brown Tuff may be due to pore-pressure generation. The application of the Mohr–Coulomb failure criterion to Atitlan 2 could not be confidently completed, as increasing normal stresses created negative internal friction and cohesion values. This indicates that another force may be present during the shearing of this material, such as pore-pressure build-up or particle crushing.

Throughout shearing, the results showed a decrease in vertical displacement (compaction) across most samples and moistures. Atitlan 2 is the only sample that shows a dilation (of 0.015 mm), which was recorded at the highest normal stress (20 kPa) at 0 wt.% moisture. However, with increasing shear distance, some granular material was lost through the gap between the two shearing rings (Supplementary Material C), and therefore, the equivalency of shear thinning and compaction was seen.

The ring shear results suggest relationships between the behaviour of the samples under varying moisture levels and normal stresses, highlighting the complexity of their mechanical response. However, Atitlan 2 does not show these relationships.

### Particle size and shape analysis

Particle crushing over time may have resulted in fundamental changes in physical particle properties, leading to changes in the shear strength of the sample. To further investigate this effect, particle size and shape (sphericity and symmetry; Table 2), analysis were completed before and after the ring shear experiments (Fig. 8).

Brown Tuff and Taupo 1 showed no apparent change in particle size distribution (PSD) following ring shear experiments, with before and after results. There was also no meaningful change in mean sphericity or symmetry values, which showed a < 0.3% difference compared to the unsheared sample.

Interestingly, Atitlan 2 shows the most significant change in PSD following ring shear, becoming finer-grained after the experiments (Fig. 9). On the analysis of the shape data, the mean sphericity and symmetry values after 0 and 1 wt.% shearing show a 1% reduction (i.e., more angular and asymmetrical) compared to the un-sheared sample. These results indicate that particle crushing occurred in the Atitlan 2 sample during the experiments. This may have affected the geomechanical properties of the material and may be the cause of the reduced shear strength results for Atitlan 2. This is interesting and could be due to the composition of the material. Previous work by Walding et al. (in press) noted that the Atitlan sample in fluidisation experiments showed no significant change in gas escape morphologies with the addition of moisture. This suggests that perhaps the

**Table 2** Material properties of both pyroclastic and cornstarch material. These include logarithmic particle size mean and particle size median, particle range, fines content (< 63 μm), and geometric mean (ϕ). The method of moments is employed for calculating Mean, Sorting, Sphericity, Symmetry, Skewness, and Kurtosis. The Sauter mean diameter is calculated following Breard et al. (2019). Material properties explored further in Walding et al. 2023; in press. The table is ordered by particle size mean

| Material | Particle Size Mean ($\bar{x}$)Ø | Particle Size Median Ø | Particle Size Range (μm) | Fines Content (%) | Sorting Index ($\sigma_I$)Ø | Sorting ($\sigma_G$) | Sphericity | Symmetry | Skewness ($Sk$)Ø | Kurtosis ($K$)Ø | Sauter Mean (mm) | Geometric Mean (μm) |
|---|---|---|---|---|---|---|---|---|---|---|---|---|
| Cornstarch | 4.8 | 4.8 | 5–340 | 96.17 | 0.595 | Moderately Well Sorted | 0.84 | 0.91 | −0.3 | 4.3 | 0.02 | 35.4 |
| Tung 1 | 3.8 | 3.7 | 2.5–297.3 | 35.76 | 0.428 | Well | 0.77 | 0.88 | 1.9 | 17.0 | 0.06 | 72.9 |
| Brown Tuff | 3.6 | 3.4 | 1—1260 | 29.35 | 1.240 | Poorly Sorted | 0.81 | 0.88 | 0.5 | 3.9 | 0.05 | 85.2 |
| Colima | 3.5 | 3.6 | 10—1000 | 84.39 | 1.453 | Poorly Sorted | 0.72 | 0.86 | −0.5 | 2.6 | 0.04 | 90.3 |
| Atitlan 2 | 3.5 | 3.8 | < 20—1780 | 40.57 | 1.501 | Poorly Sorted | 0.83 | 0.91 | −0.9 | 3.2 | 0.02 | 92.4 |
| Atitlan 1 | 2.8 | 3.1 | 2—2000 | 66.03 | 2.426 | Very Poorly Sorted | 0.76 | 0.89 | 0.1 | 2.0 | 0.02 | 97.2 |
| Tung 4 | 2.7 | 2.7 | 20–650 | 0.15 | 0.252 | Very well | 0.84 | 0.87 | 0.1 | 8.5 | 0.01 | 153.5 |
| Taupo 2 | 2.4 | 2.3 | < 20—2000 | 52.23 | 0.979 | Moderately Sorted | 0.70 | 0.86 | −0.5 | 4.1 | 0.04 | 195.8 |
| Taupo 1 | 2.1 | 2.2 | < 20—2000 | 38.90 | 1.158 | Poorly Sorted | 0.75 | 0.87 | −0.5 | 3.3 | 0.04 | 234.6 |
| Tung 5 | 1.6 | 1.6 | 10–1000 | 0.09 | 0.758 | Moderate | 0.80 | 0.87 | −0.1 | 2.5 | 0.02 | 347.3 |
| Tung 6 | 0.8 | 0.8 | 10—1000 | 0.04 | 0.445 | Well | 0.79 | 0.87 | 0.6 | 8.3 | 0.03 | 557.1 |

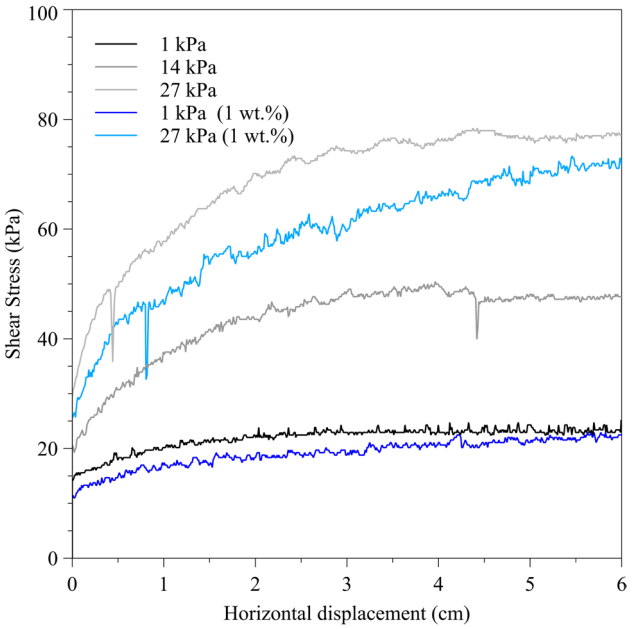


**Fig. 7** Direct shear box test of Tung 4 at 0 wt.% (black) and 1 wt.% (blue) moisture contents. Note that the yield stress was not reached. See Supplementary Material E

Atitlan material has $H_20$ scavenging minerals present or has been hydrothermally altered, ultimately leading to the weakening of the particles, resulting in increased crushing of material. This observation would benefit from future work into the nature of hydrothermally altered ash material and moisture.

## Drop tests

Drop tests were carried out to determine whether the rheological properties of ash change at high moisture contents due to the effect known as "shear-thickening" (as seen in cornstarch material). We hypothesise that where ash pellet layers are preserved beneath lithic breccia lithofacies, the impact and shear from the large lithic blocks may induce shear thickening. The increased viscosity may increase the material's resistance and, therefore, develop a "protection" from the erosion of the dense granular current.

The drop test on cornstarch (96% fine content) at 80 wt.% moisture demonstrated non-Newtonian and shear-thickening behaviour. The steel ball dropped at a speed of 0.16 cm/s, impacting the surface of the mixture and bouncing to a height of 0.55 cm (Supplementary Material F). In the pyroclastic material, two samples showed these same shear thickening behaviours (i.e., bouncing off the substrate deposit) correlated to high fine content.

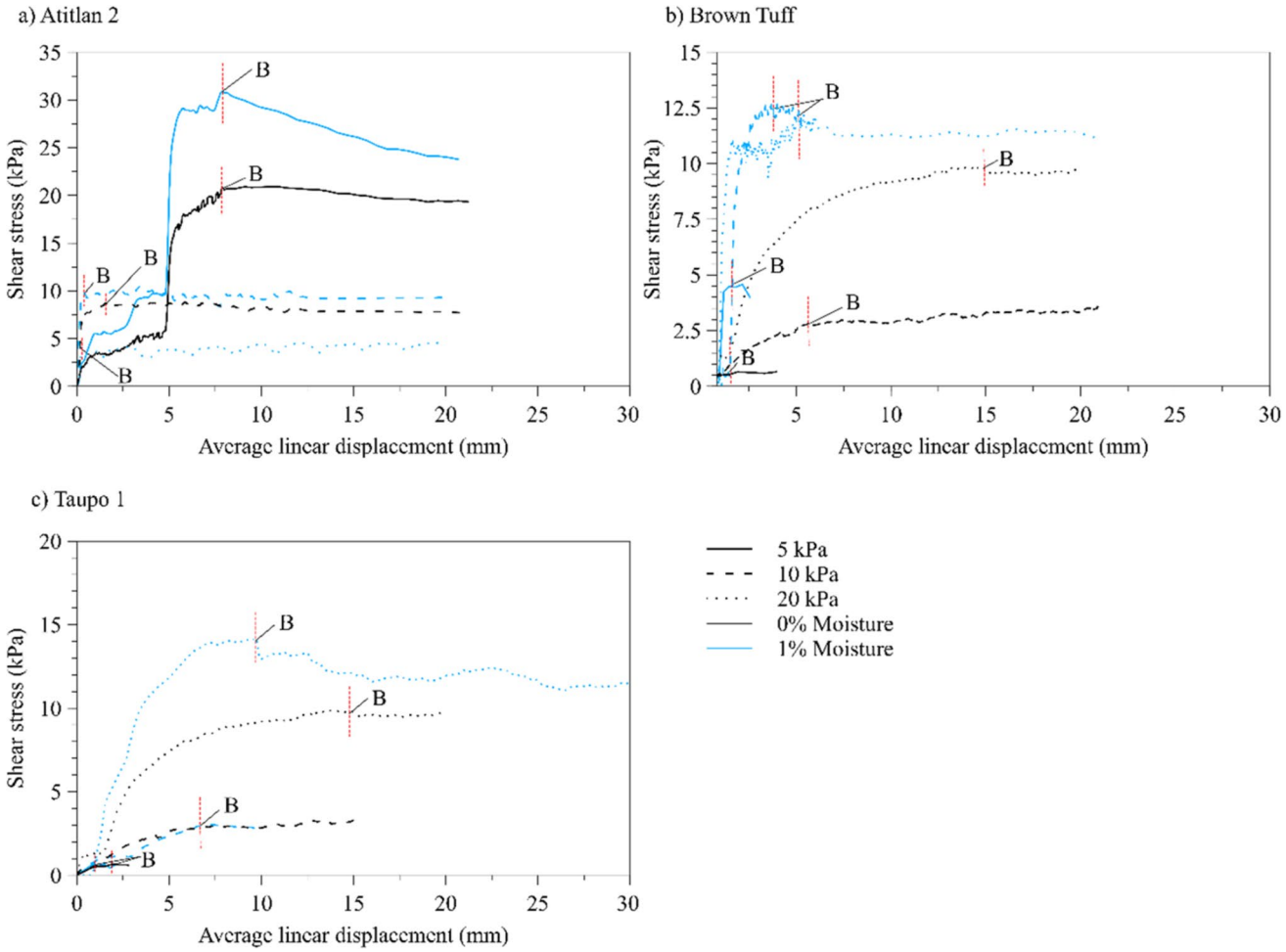


**Fig. 8** **a** Atitlan 2, **b** Brown Tuff, and **c** Taupo 1 shearing profiles of material at varying moisture contents (0 and 1 wt.%). (B) shows peak stress, and a dashed red line highlights the yield stress and separates areas of elastic response (left-hand side of the graph) and plastic hardening (right-hand side of the graph)

The results for pyroclastic materials show that with sufficiently high wt.% moisture, Atitlan 1 (~ 40 wt.%, 66.03% fine content), Colima (~ 25 wt.%, 84.39% fine content), Taupo 1 (~ 50 wt.%, 38.9% fine content), and Taupo 2 (~ 70 wt.%, 52.23% fine content) all show evidence of shear thickening (i.e., a reducing ball penetration depth with increasing moisture and in some cases show the ball bouncing off the surface; Fig. 10, Supplementary Material F). At 50 wt.%, the ball bounced and reached a height of 0.6 cm for the Taupo 1 sample and ~ 0.6 cm for the 70 wt.% Taupo 2 sample (Supplementary Material F).

When moisture levels were increased above these percentages for each sample, the ball completely penetrated the saturated deposit with little resistance (Fig. 10d).

Shear thickening behaviours were associated only with some finer materials at a limited moisture range. Tung 6 (particle size mean 0.833 ϕ, 0.04% fine content) did not show shear thickening in any experiment; at all moistures tested (30–40 wt.%), the ball moved straight through the material (Supplementary Material F).

These results demonstrate the ability of pyroclastic material to exhibit changes in strength at varying moisture ranges, dependent upon particle characteristics. The ball moves directly through all samples' deposits at dry or low moisture contents under loose conditions (e.g., Fig. 10b). At high moisture levels (Atitlan 1, > 50 wt.%; Colima, 30 wt.%; Taupo 1, > 60 wt.%; Taupo 2, > 80 wt.%), the material becomes a particle suspension, where the granular material is dominated by particle–fluid interactions (Sosio and Crosta 2009) and the ball moves straight through the deposit (Fig. 10d). Some pyroclastic materials, as seen in Taupo 1 and 2, can show shear-thickening behaviour (Fig. 10c). This is not the case for Tung 6, probably due to its lack of fines content. When impacted or sheared, a shear-thickening material stiffens, which can result in resistance to deformation or penetration (as indicated in our results).

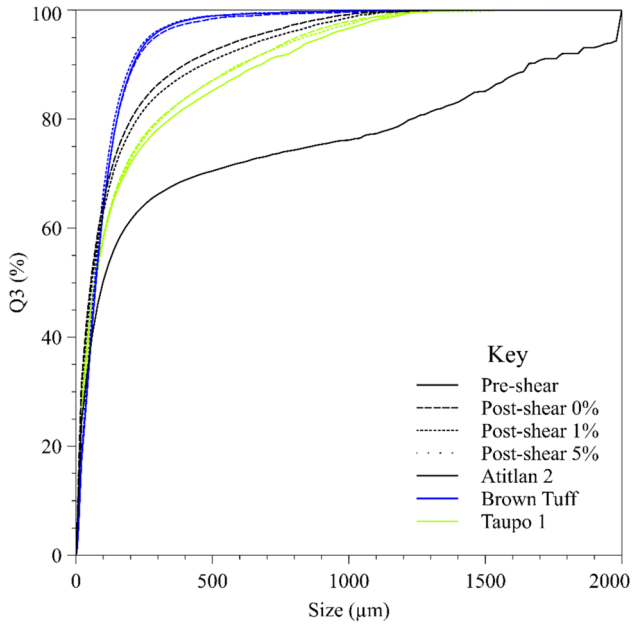


**Fig. 9** Particle size analysis of material before and after the ring shear experiments

## Discussion

### Dry deposit

The dry deposit environment is a baseline comparison since it represents a deposit not influenced by moisture (i.e., lacking accretionary lapilli or ash pellets). A dry ash substrate can form from ash fallout originating from an eruption plume, the fallout of a dry co-ignimbrite cloud or the deposition of a dilute PDC (e.g., Fig. 3a, 11). In such cases, the shear strength and cohesivity of the deposit are low. Variations in shear strength will be primarily influenced by particle packing, particle density and fine content (Roberts et al. 1998; Kimiaghalam et al. 2016). Shear strength and cohesivity will be affected by fines content and grain size, resulting in the formation of Van der Waals or electrostatic forces between particles.

In the field, ash layers that were interpreted to be dry did not show sharp, upper contacts with overriding PDC deposits, nor did they display peeling features or any other features indicative of cohesivity or shear strength. The loose nature of recently deposited ash layers makes them vulnerable to erosion by subsequent PDC activity. As a result, even when thin ash layers are deposited that could record a hiatus and delineate a flow unit (i.e., co-ignimbrite or plume fallout), their low preservation potential makes them unlikely to be recorded in volcanic stratigraphy—resulting in cryptic or missed layers (Fig. 11). Additionally, the erosion of the dry substrate may lead to entrainment and bulking of the overriding current, potentially increasing run-out distances and increasing the hazard risk (Bernard et al. 2014).

### Moisture-affected deposits

A moisture-affected deposit is characterised by the influence of moisture, as inferred by the presence of accretionary lapilli and ash pellets. Ash pellets can form from a moist co-ignimbrite cloud or when raindrops interact with ash particles (Fig. 11, Brown et al. 2012; Diaz-Vecino et al. 2022). Consequently, resulting deposits may exhibit a range of moisture contents, from low to potentially saturated levels, either due to the presence of a high concentration of ash pellets or from direct rainfall on the aggrading deposits. Accretionary lapilli is formed by the lofting and cycling of ash pellets between hotter, lower areas, and moister, cooler upper areas of a PDC, which leads to the accretion of thin concentric ash layers (Reimer 1983; Schumacher and Schmincke 1995; Brown et al. 2012; Diaz-Vecino et al. 2023). The final deposits are interpreted as being indicative of general low-moisture conditions. Given that PDCs are typically hot, it is unlikely that these deposits would be uniformly moist or

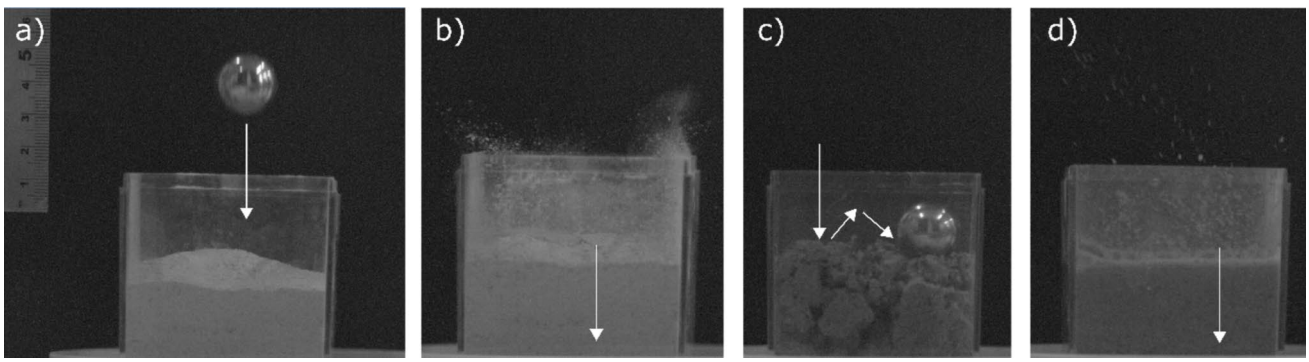


**Fig. 10** Drop test completed on Taupo 1 sample at **b** 0 wt.% moisture, **c** 50 wt.% moisture, and **d** 60 wt.%. Arrows show the movement of the ball from **a** falling, **b** and **d** moving through the material and **c** showing the bouncing movement of the ball on impact with the deposit

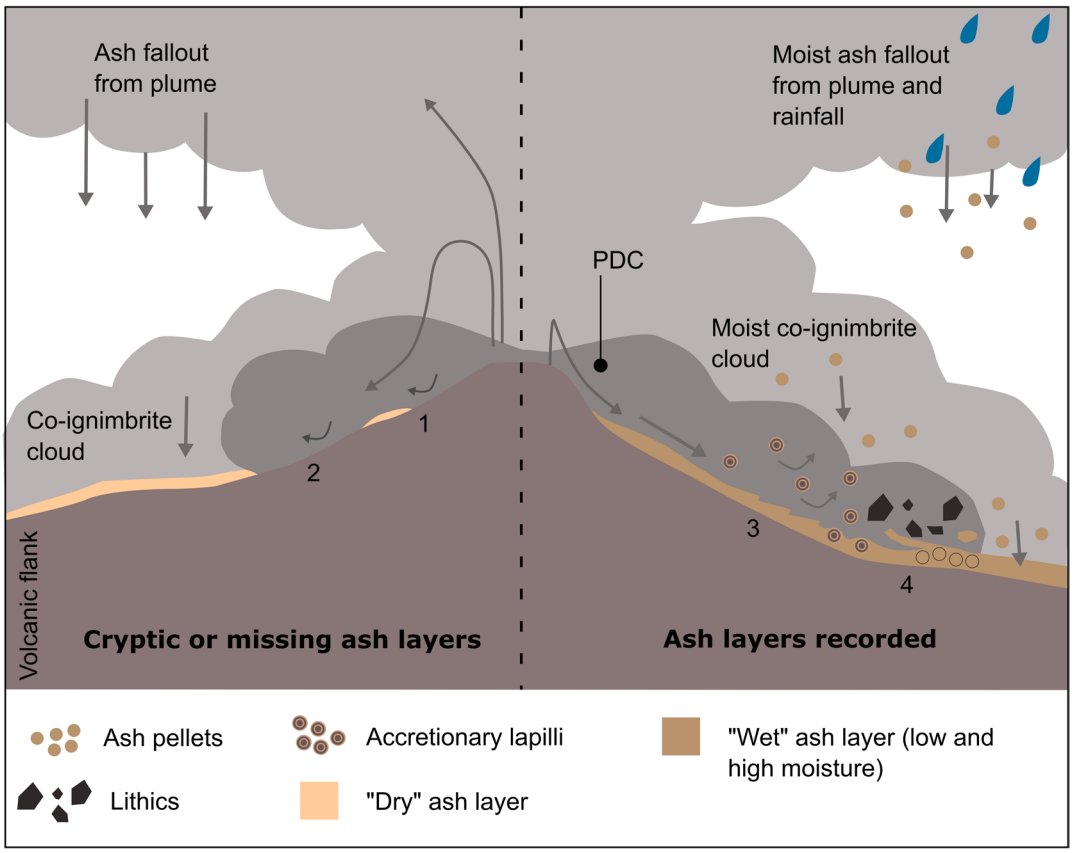


**Fig. 11** Schematic showing dry (left) and wet (right) ash layers forming from dry and moist plume fallout, co-ignimbrite fallout and dilute PDC deposition. At the dry locality, a subsequent PDC entrains (1) the loose ash material, possibly leading to bulking (2) in the current. The final deposit shows a cryptic or missing ash layer. In the wet scenario, moisture in the substrate is inferred by the presence of accretionary lapilli and ash pellets, which lead to an overall more cohesive deposit of greater shear strength (3). Furthermore, where lithics are present (4), high moisture substrates can experience shear thickening. This results in the preservation of "wet" ash layers, which are recorded

saturated, leading instead to spatial variations in moisture content. Furthermore, the presence of water can facilitate salt and mineral precipitation at the particle boundaries, accretionary lapilli can be strong, and energy exerted on them (i.e., from the collision with other particles) can result in their fragmentation or complete disaggregation (Mueller et al. 2017).

In the field, ash layers rich in accretionary lapilli sometimes displayed stepped erosive contacts, where the contact sheared through them, or more diffuse contacts, where the contact wrapped around protruding accretionary lapilli. For the accretionary lapilli to be sheared through, they and the surrounding unconsolidated ash must possess similar sufficient inherent strength to resist disaggregation and erosion despite having only recently formed. Additionally, the presence of protruding accretionary lapilli that were not plucked out by the overriding current, suggests that the lapilli are strong (Fig. 11). Laboratory experiments with low moisture conditions support these field observations, where moisture increase from 0 to 1 wt.% in pyroclastic material increases the yield strength and, therefore, resistance to shear (Fig. 11).

In contrast, ash pellet layers often formed sharp contacts with overlying lithic-rich deposits and, in some cases, were seen to be 'lifted', 'peeled up' or incorporated as clasts, indicating a greater shear strength within the deposit, allowing for coherent remobilisation of these layers. These features are reminiscent of deformed laminations and rip-up clasts of mud layers seen within turbidite sequences. Such features occur in turbidite sequences when cohesive sediments, like clay, bind together and are subsequently eroded and transported (Allen 1982; Li et al. 2017; Yang et al. 2024).

The erosion of mud-rich sediments requires a critical shear stress to initiate substrate erosion (Chen et al. 2021a, b). Particle size plays a crucial role in influencing a material's erosional potential; for example, clay-rich materials exhibit greater cohesion compared to sand-dominated, granular materials. In addition, experimental studies have demonstrated that cohesive sediments erode as aggregates under low bed shear stresses or as 'clasts' of material under

higher shear stresses (Sanford and Maa 2001; Le Hir et al. 2011; Chen et al. 2018; 2021a, b, and references therein).

The results from the shear experiments (Fig. 8b, c) show that increasing moisture (1 wt.%) led to an increase in the yield strength. The elastic limit is reached in less time than the dry material in the 1 wt.% substrates (Brown Tuff and Taupo 1). This indicates that the 1% material is deforming over shorter periods of time, but with more yield strength required to do so than material at lower moisture content. The separation between plastic and elastic deformation may also explain the remobilisation structures seen. For example, the elastic deformation (i.e., connected to the base and being "peeled" up) of the feature in Fig. 7 and the more plastic deformation (i.e., the brittle separation from the underlying substrate) of feature A in Fig. 6. Furthermore, at high moisture contents (25–70 wt.%), the drop tests revealed that a ball will impact and bounce off a deposit, resulting in less penetration. This reveals compelling evidence of shear thickening in a high-moisture pyroclastic material, leading to the dynamic preservation of high-moisture layers in high-stress environments. This behaviour, commonly seen in dense suspensions of solid particles, illustrates the complex rheological response of ash deposits, which can transition from easy flow at low shear rates (as determined by the shear experiments) to solid-like resistance at higher shear stresses (drop tests). In volcanic successions, this process may explain the resistance of thin ash pellet layers to erosion by more significant, caldera-forming deposits, such as lithic breccia.

## Implications for interpreting PDC stratigraphy and hazard

This work demonstrates the influence of moisture on the preservation of ash layers that can be important marker horizons (Fig. 1) and finds that ash layers formed in low or high moisture conditions are more likely to be preserved than those formed in dry conditions (Fig. 11).

These findings have important implications for interpreting ash layers in volcaniclastic sequences, which can record episodes of PDC hiatus and delineate flow units. A lack of understanding of the preservation potential of an ash layer could lead to an overestimation or underestimation of the number of flow units in a deposit, relevant to interpretations of the location of PDC hazard through time. Furthermore, understanding the likelihood of erosion and incorporation of a fine-grained ash substrate into a PDC is non-trivial; the entrainment of dry, loose material can promote flow bulking of PDCs, resulting in increased flow mobility, higher velocities and extended runout distances (Iverson 2012; Bernard et al. 2014).

Future research should focus on understanding deposit variability in order to determine how natural changes in the substrate affect entrainment, thereby contributing to current bulking and the removal of key deposit layers. Additionally, further investigation into the rheological behaviour of pyroclastic materials under varying moisture and shear conditions would provide a more precise understanding of shear thickening behaviour. This is important in understanding the erosion processes that might lead to flow-bulking and associated modifications to flow hazard. Finally, when reassessing past deposits and conducting future studies, it will be crucial to consider the role of cohesion in layer preservation and incorporate this factor into stratigraphic field interpretations.

**Supplementary Information** The online version contains supplementary material available at https://doi.org/10.1007/s00445-025-01821-4.

**Acknowledgements** Dr Richard Brown (University of Durham) is acknowledged for sharing knowledge, time, and locations. Thank you to Dr Anna Bird for your insightful comments on this piece of work. We appreciate all pyroclastic material donations that have been shipped and sent to us to complete this work (Gert Lube, Ermanno Brosch, Ulli Kueppers and Tom Johnston). Thank you to Kirk Handley and Gary Martin for the equipment and advice. Finally, we are grateful to Baptiste Penlou and Adrian Pittari for their thoughtful comments and reviews.

**Funding** This study was funded by the EU Horizon 2020 programme (Project GEOSTICK 712525). The British Sedimentological Research Group provided partial financial support for the award of the Gillian Harwood Fund, which facilitated the success of the Tenerife field expedition.

## Declarations

**Competing interests** The authors declare no competing interests.



## References

Alias R, Kasa A, Taha MR (2014) Particle size effect on shear strength of granular materials in direct shear test. J Civ Environ Eng 8(11):1048–1051

Allen J (1982) Sedimentary structures: Their character and physical basis, vol 2. Elsevier, Amsterdam

Álvarez JAC, Carrasco-Núñez G (2019) Anatomy of the Xáltipan ignimbrite at Los Humeros Volcanic Complex; the largest eruption of the Trans-Mexican Volcanic Belt. J Volcanol Geotherm Res 106755. https://doi.org/10.1016/j.jvolgeores.2019.106755

Auker MR, Sparks RSJ, Siebert L, Crosweller HS, Ewert J (2013) A statistical analysis of the global historical volcanic fatalities record. J Appl Volcanol 2:1–24. https://doi.org/10.1186/2191-5040-2-2

Báez W, de Silva S, Chiodi A, Bustos E, Giordano G, Arnosio M, Suzaño N, Viramonte JG, Norini G, Groppelli G (2020) Pulsating flow dynamics of sustained, forced pyroclastic density currents: insights from a facies analysis of the Campo de la Piedra Pómez ignimbrite, southern Puna. Argentina Bull Volcanol 82(7):53. https://doi.org/10.1007/s00445-020-01385-5

Bernard J, Kelfoun K, Le Pennec JL et al. (2014) Pyroclastic flow erosion and bulking processes: comparing field-based vs. modeling results at Tungurahua volcano, Ecuador. Bull Volcanol 76:858. https://doi.org/10.1007/s00445-014-0858-y

Bishop AW, Green GE, Garga VK, Andresen A, Brown JD (1971) A new ring shear apparatus and its application to the measurement of residual strength. Geotechnique 21(4):273–328. https://doi.org/10.1680/geot.1971.21.4.273

Blott SJ, Pye K (2001) GRADISTAT: a grain size distribution and statistics package for the analysis of unconsolidated sediments. Earth Surf Process Landf 26:1237–1248. https://doi.org/10.1002/esp.261

Brand BD, Mackaman-Lofland C, Pollock NM, Bendaña S, Dawson B, Wichgers P (2014) Dynamics of pyroclastic density currents: conditions that promote substrate erosion and self-channelization—Mount St Helens, Washington (USA). J Volcanol Geotherm Res 276:189–214. https://doi.org/10.1016/j.jvolgeores.2014.01.007

Branney M, Kokelaar P (2002) Pyroclastic density currents and the sedimentation of ignimbrites. Geological Society, London. https://doi.org/10.1144/GSL.MEM.2003.027

Branney MJ, Kokelaar P (1992) A reappraisal of ignimbrite emplacement: progressive aggradation and changes from particulate to non-particulate flow during emplacement of high-grade ignimbrite. Bull Volcanol 54(6):504–520. https://doi.org/10.1007/bf00301396

Breard E, Jones J, Fullard L, Lube G, Davies C, Dufek J (2019) The permeability of volcanic mixtures—implications for pyroclastic currents. J Geophys Res Solid Earth 124(2):1343–1360. https://doi.org/10.1029/2018JB016544

Brown R, Barry T, Branney M, Pringle M, Bryan S (2003) The Quaternary pyroclastic succession of southeast Tenerife, Canary Islands: explosive eruptions, related caldera subsidence, and sector collapse. Geol Mag 140:265. https://doi.org/10.1017/S0016756802007252

Brown RJ, Bonadonna C, Durant AJ (2012) A review of volcanic ash aggregation. Phys Chem Earth Parts a/b/c 45–46:65–78. https://doi.org/10.1016/j.pce.2011.11.001

Brown RJ, Branney MJ (2004) Event-stratigraphy of a caldera-forming ignimbrite eruption on Tenerife: the 273 ka Poris Formation. Bull Volcanol 66:392–416. https://doi.org/10.1007/s00445-003-0321-y

Brown RJ, Branney MJ (2013) Internal flow variations and diachronous sedimentation within extensive, sustained, density-stratified pyroclastic density currents flowing down gentle slopes, as revealed by the internal architectures of ignimbrites on Tenerife. Bull Volcanol 75(7):1–24. https://doi.org/10.1007/s00445-013-0727

Brown RJ, Branney MJ, Maher C, Dávila-Harris P (2010) Origin of accretionary lapilli within ground-hugging density currents: evidence from pyroclastic couplets on Tenerife. GSA Bull 122(1–2):305–320. https://doi.org/10.1130/B26449.1

Buckland HM, Saxby J, Roche M, Meredith P, Rust AC, Cashman KV, Engwell SL (2021) Measuring the size of non-spherical particles and the implications for grain size analysis in volcanology. J Volcanol Geotherm Res 415:107257. https://doi.org/10.1016/j.jvolgeores.2021.107257

Bursik M, Woods A (1996) The dynamics and thermodynamics of large ash flows. Bull Volcanol 58:175–193. https://doi.org/10.1007/s004450050134

Camuffo D (2019) Theoretical grounds for humidity. In: Microclimate for Cultural Heritage. Elsevier, pp 43–59. https://doi.org/10.1016/B978-0-444-64106-9.00003-1.

Cas RAF, Wright JV (1987). Volcanic Successions Modern and Ancient. https://doi.org/10.1007/978-94-009-3167-1

Cavazos-Álvarez JA, Carrasco-Núñez G, Dávila-Harris P, Peña D, Jáquez A, Arteaga D (2020) Facies variations and permeability of ignimbrites in active geothermal systems; case study of the Xáltipan ignimbrite at Los Humeros Volcanic Complex. J South Am Earth Sci 104:102810. https://doi.org/10.1016/j.jsames.2020.102810

Charbonnier SJ, Garin F, Rodríguez LA et al (2023) Unravelling the dynamics and hazards of the June 3rd, 2018, pyroclastic density currents at Fuego volcano (Guatemala). J Volcanol Geotherm Res 436:107791. https://doi.org/10.1016/j.jvolgeores.2023.107791

Chen D, Melville B, Zheng J, Wang Y, Zhang C, Guan D, Chen C (2021a) Pickup rate of non-cohesive sediments in low-velocity flows. J Hydraul Res 60(1):125–135. https://doi.org/10.1080/00221686.2020.1871430

Chen D, Wang Y, Melville B, Huang H, Zhang W (2018) Unified formula for critical shear stress for erosion of sand, mud, and sand-mud mixtures. J Hydraul Eng 144(8). https://doi.org/10.1061/(ASCE)HY.1943-7900.0001489.

Chen D, Zheng J, Zhang C, Guan D, Li Y, Wang Y (2021b) Critical shear stress for erosion of sand-mud mixtures and pure mud. Front Mar Sci 8:713039. https://doi.org/10.3389/fmars.2021.713039

Cole PD, Calder ES, Druitt TH et al (1998) Pyroclastic flows generated by gravitational instability of the 1996–97 Lava Dome of Soufriere Hills Volcano. Montserrat Geophys Res Lett 25(18):3425–3428. https://doi.org/10.1029/98GL01510

Cole PD, Calder ES, Sparks RSJ et al (2002) Deposits from dome-collapse and fountain-collapse pyroclastic flows at Soufriere Hills Volcano, Montserrat. Geol Soc Mem 21:231–262. https://doi.org/10.1144/gsl.mem.2002.021.01.11

Crawford NC, Popp LB, Johns KE, Caire LM, Peterson BN, Liberatore NW (2013) Shear thickening of corn starch suspensions: does concentration matter? J Colloid Interface Sci 396:83–89. https://doi.org/10.1016/j.jcis.2013.01.024

Dartevelle S, Ernst GGJ, Stix J, Bernard A (2002) Origin of the Mount Pinatubo climactic eruption cloud: implications for volcanic hazards and atmospheric impacts. Geology 7:663

Diaz-Vecino C, Rossi E, Pollastri S et al (2023) Insights into the sticking probability of volcanic ash particles from laboratory experiments. Sci Rep 13:21188. https://doi.org/10.1038/s41598-023-47712-6

Donaldson EC, Alam W, Begum N (2013) Rock mechanics of fracturing. In: Donaldson EC, Alam W, Begum N (eds) Hydraulic fracturing explained. Gulf Publishing Company, pp 47–76. https://doi.org/10.1016/B978-1-933762-40-1.50012-X.

Douillet GA, Tsang-Hin-Sun È, Kueppers U et al (2013) Sedimentology and geomorphology of the deposits from the August 2006 pyroclastic density currents at Tungurahua volcano. Ecuador Bull Volcanol 75:765. https://doi.org/10.1007/s00445-013-0765-7

Dowey N, Williams R (2022) Simultaneous fall and flow during pyroclastic eruptions: a novel proximal hybrid facies. Geology 50(10):1187–1191. https://doi.org/10.1130/G50169.1

Dowey NJ, Brown RJ, Kokelaar BP (2024) Counting currents: resolving contradictory records of eruption history created by unsteady pyroclastic density current dynamics. EarthArXiv. https://doi.org/10.31223/X5W42M.

Druitt TH, Mellors RA, Pyle DM, Sparks RSJ (1989) Explosive volcanism on Santorini. Greece Geol Mag 126(02):95. https://doi.org/10.1017/s0016756800006270

Edgar CJ, Wolff JA, Nichols HJ et al (2002) A complex Quaternary ignimbrite-forming phonolitic eruption: the Poris Member of the Diego Hernández Formation (Tenerife, Canary Islands). J

Volcanol Geotherm Res 118(1–2):99–130. https://doi.org/10.1016/S0377-0273(02)00252-4
Edgar CJ, Wolff JA, Olin PH et al (2007) The late Quaternary Diego Hernandez Formation, Tenerife: volcanology of a complex cycle of voluminous explosive phonolitic eruptions. J Volcanol Geotherm Res 160(1–2):59–85. https://doi.org/10.1016/j.jvolgeores.2006.06.001
Eychenne J, Pennec JLL, Troncoso L, Gouhier M, Nedelec JM (2012) Causes and consequences of bimodal grain-size distribution of tephra fall deposited during the August 2006 Tungurahua eruption (Ecuador). Bull Volcanol 74:187–205. https://doi.org/10.1007/s00445-011-0517-5
Fisher RV (1979) Models for pyroclastic surges and pyroclastic flows. J Volcanol Geotherm Res 6:305–318. https://doi.org/10.1016/0377-0273(79)90008-8
Geldart D (1973) Types of gas fluidization. Powder Technol 7:285–292. https://doi.org/10.1016/0032-5910(73)80037-3
Gilbert JS, Lane SJ (1994) The origin of accretionary lapilli. Bull Volcanol 56:398–411. https://doi.org/10.1007/BF00326465
Grabowski RC, Droppo IG, Wharton G (2011) Erodibility of cohesive sediment: the importance of sediment properties. Earth Sci Rev 105:101–120. https://doi.org/10.1016/j.earscirev.2011.01.008
Hall M, Mothes P, Ramon P, Arellano S, Barba D, Palacios P (2007) Dense pyroclastic flows of the 16–17 August 2006 eruption of Tungurahua Volcano. Ecuador, AGU Joint Assembly, Acapulco, Mexico
Houghton B, White JDL, Van Eaton AR (2015) Phreatomagmatic and related eruption styles. In: Sigurdsson H, Houghton B, Rymer H, Stix J, McNutt S (eds) The Encyclopedia of Volcanoes. Elsevier, pp 537–552. https://doi.org/10.1016/B978-0-12-385938-9.00030-4
Hurwitz S, Kipp KL, Ingebritsen SE, Reid ME (2003) Groundwater flow, heat transport, and water table position within volcanic edifices: implications for volcanic processes in the Cascade Range. J Geophys Res 108(B12). https://doi.org/10.1029/2003jb002565
Inman DL (1952) Measures for describing the size distribution of sediments. J Sed Res 22:125–145. https://doi.org/10.1306/D42694DB-2B26-11D7-8648000102C1865D
Iverson RM (2012) Elementary theory of bed-sediment entrainment by debris flows and avalanches. J Geophys Res 117(F3). https://doi.org/10.1029/2011JF002189
Jiang X, Cui P, Ge Y (2015) Effects of fines on the strength characteristics of mixtures. Eng Geol 198:78–86. https://doi.org/10.1016/j.enggeo.2015.09.011
Keaton JR (2018) Shear Modulus. In: Bobrowsky PT, Marker B (eds) Encyclopedia of Engineering Geology. Encyclopedia of Earth Sciences Series. Springer, Cham. https://doi.org/10.1007/978-3-319-73568-9_256
Kelfoun K, Samaniego P, Palacios P, Barba D (2009) Testing the suitability of frictional behaviour for pyroclastic flow simulation by comparison with a well-constrained eruption at Tungurahua volcano (Ecuador). Bull Volcanol 71:1057–1075. https://doi.org/10.1007/s00445-009-0286-6
Kim TH, Sture S (2008) Capillary-induced tensile strength in unsaturated sands. Can Geotech J 45:726–737. https://doi.org/10.1139/T08-017
Kimiaghalam N, Clark SP, Ahmari H (2016) An experimental study on the effects of physical, mechanical, and electrochemical properties of natural cohesive soils on critical shear stress and erosion rate. Int J Sediment Res 31:1–15. https://doi.org/10.1016/j.ijsrc.2015.01.001
Le Hir P, Cayocca F, Waeles B (2011) Dynamics of sand and mud mixtures: a multiprocess-based modelling strategy. Cont Shelf Res 31:135–149. https://doi.org/10.1016/j.csr.2010.12.009
Li S, Li S, Shan X, Gong C, Yu X (2017) Classification, formation, and transport mechanisms of mud clasts. Int Geol Rev 59:1609–1620. https://doi.org/10.1080/00206814.2017.1287014
Liu EJ, Cashman KV, Rust AC (2015) Optimising shape analysis to quantify volcanic ash morphology. GeoResJ 8:14–30. https://doi.org/10.1016/j.grj.2015.09.001
Liu H, Wang C, Wu D, Liu X, Zhang Z (2022) Deformation and critical dynamic stress for compacted volcanic ash subjected to monotonic and dynamic loads. Constr Build Mater 358. https://doi.org/10.1016/j.conbuildmat.2022.129454
Lowe DJ, Pittari A (2021) The Taupō eruption sequence of AD 232 ± 10 in Aotearoa New Zealand: A retrospection. J Geography 130:117–141. https://doi.org/10.5026/jgeography.130.117
Lube G, Breard EC, Esposti-Ongaro T, Dufek J, Brand B (2020) Multiphase flow behaviour and hazard prediction of pyroclastic density currents. Nat Rev Earth Environ 1:348–365. https://doi.org/10.1038/s43017-020-0064-8
Lucchi F, Francalanci L, De Astis G, Tranne CA, Braschi E, Klaver M (2018) Geological evidence for recurrent collapse-driven phreatomagmatic pyroclastic density currents in the Holocene activity of Stromboli volcano, Italy. J Volcanol Geotherm Res. https://doi.org/10.1016/j.jvolgeores.2018.10.
Massoudi M, Mehrabadi MM (2001) A continuum model for granular materials: considering dilatancy and the Mohr-Coulomb criterion. Acta Mech 152:121–138. https://doi.org/10.1007/BF01176949
Moyer TC, Swanson DA (1987) Secondary hydroeruptions in pyroclastic-flow deposits: examples from Mount St. Helens J Volcanol Geotherm Res 32:299–319. https://doi.org/10.1016/0377-0273(87)90081-3
Mueller SB, Kueppers U, Ametsbichler J, Cimarelli C, Merrison JP, Poret M, Wadsworth FB, Dingwell DB (2017) Stability of volcanic ash aggregates and break-up processes. Sci Rep 7:7440. https://doi.org/10.1038/s41598-017-07927-w
Niroumand H (2017) Chapter 3 - Research methodology. In: Niroumand H (ed) Soil reinforcement for anchor plates and uplift response. Butterworth-Heinemann, pp 67–96
Pepin NC, Pike G, Schaefer M, Boston CM, Lovell H (2017) A comparison of simultaneous temperature and humidity observations from the SW and NE slopes of Kilimanjaro: the role of slope aspect and differential land-cover in controlling mountain climate. Global Planet Change 157:244–258. https://doi.org/10.1016/j.gloplacha.2017.08.006
Pittari A, Cas RAF, Edgar CJ, Nichols HJ, Wolff JA, Martí J (2006) The influence of palaeotopography on facies architecture and pyroclastic flow processes of a lithic-rich ignimbrite in a high gradient setting: the Abrigo Ignimbrite, Tenerife. Canary Islands J Volcanol Geotherm Res 152(3–4):273–315. https://doi.org/10.1016/j.jvolgeores.2005.10.007
Reimer TO (1983) Accretionary lapilli in volcanic ash falls: physical factors governing their formation. Coated grains. Springer, Berlin Heidelberg, pp 56–68
Roberts J, Jepsen R, Gotthard D, Lick W (1998) Effects of particle size and bulk density on erosion of quartz particles. J Hydraul Eng 124(12):1261–1267. https://doi.org/10.1061/(asce)0733-9429(1998)124:12(1261)
Roche O, Niño Y, Mangeney A, Brand B, Pollock N, Valentine GA (2013) Dynamic pore-pressure variations induce substrate erosion by pyroclastic flows. Geology 41(10):1107–1110. https://doi.org/10.1130/G34668.1
Rowley P, Williams R, Johnson M, Johnston T, Dowey N, Parsons D, Provost A, Roche O, Smith G, Walding N (2023) EarthARXiv. EarthARXiv [Preprint]. https://doi.org/10.31223/X51M32
Sanford L, Maa JPY (2001) A unified erosion formulation for fine sediments. Mar Geol 179(1–2):9–23. https://doi.org/10.1016/S0025-3227(01)00201-8
Schindelin J, Arganda-Carreras I, Frise E, Kaynig V, Longair M, Pietzsch T et al (2012) Fiji: an open-source platform for biological-image analysis. Nat Methods 9(7):676–682. https://doi.org/10.1038/nmeth.2019

Schumacher R, Schmincke HU (1995) Models for the origin of accretionary lapilli. Bull Volcanol 56:626–639. https://doi.org/10.1007/BF00301467

Self S, Sparks RSJ (1978) Characteristics of widespread pyroclastic deposits formed by the interaction of silicic magma and water. Bull Volcanol 41:196–212

Sheng D, Zhou A, Fredlund DG (2011) Shear strength criteria for unsaturated soils. Geotech Geol Eng 29:145–159. https://doi.org/10.1007/s10706-009-9276-x

Shimizu HA, Koyaguchi T, Suzuki YJ (2023) Dynamics and deposits of pyroclastic density currents in magmatic and phreatomagmatic eruptions revealed by a two-layer depth-averaged model. Geophys Res Lett 50(16):616. https://doi.org/10.1029/2023GL104616

Sigurdsson H, Carey S (1989) Plinian and co-ignimbrite tephra fall from the 1815 Tambora eruption. Bull Volcanol 51(4):243–270. https://doi.org/10.1007/BF01073515

Sigurdsson H, Carey SN, Espindola JM (1984) The 1982 eruptions of El Chichón Volcano, Mexico: stratigraphy of pyroclastic deposits. J Volcanol Geotherm Res 23(1–2):11–37. https://doi.org/10.1016/0377-0273(84)90055-6

Silva Parejas C, Druitt TH, Robin C et al (2010) The Holocene Pucón eruption of Volcán Villarrica, Chile: deposit architecture and eruption chronology. Bull Volcanol 72:677–692. https://doi.org/10.1007/s00445-010-0348-9

Smith NJ, Kokelaar BP (2013) Proximal record of the 273 ka Poris caldera-forming eruption, Las Cañadas. Tenerife Bull Volcanol 75:768. https://doi.org/10.1007/s00445-013-0768-4

Sosio R, Crosta G (2009) Rheology of concentrated granular suspensions and possible implications for debris flow modelling. Water Resour Res 45(3). https://doi.org/10.1029/2008WR006920

Sparks R, Gardeweg M, Calder E et al (1997) Erosion by pyroclastic flows on Lascar Volcano, Chile. Bull Volcanol 58:557–565. https://doi.org/10.1007/s004450050162

Sparks RSJ (1976) Grain size variations in ignimbrites and implications for the transport of pyroclastic flows. Sedimentology 23(2):147–188. https://doi.org/10.1111/j.1365-3091.1976.tb00045.x

Sparks RSJ, Self S, Walker GPL (1973) Products of ignimbrite eruptions. Geology 1(3):115–118. https://doi.org/10.1130/0091-7613(1973)12.0.CO;2

Sparks RSJ, Walker GPL (1977) The significance of vitric-enriched air-fall ashes associated with crystal-enriched ignimbrites. J Volcanol Geotherm Res 2(4):329–341. https://doi.org/10.1016/0377-0273(77)90019-1

Sulpizio R, Dellino P, Doronzo DM, Sarocchi D (2014) Pyroclastic density currents: state of the art and perspectives. J Volcanol Geotherm Res 283:36–65. https://doi.org/10.1016/j.jvolgeores.2014.06.014

Telling J, Dufek J, Shaikh A (2013) Ash aggregation in explosive volcanic eruptions. Geophys Res Lett 40(10):2355–2360. https://doi.org/10.1002/grl.50376

Vecino MCD, Rossi E, Freret-Logeril V, Fries A, Gabellini P, Lemus J, Pollastri S, Poulidis AP, Iguchi M, Bonadonna C (2022) Aerodynamic characteristics and genesis of aggregates at Sakurajima Volcano, Japan. Sci Rep 14. https://doi.org/10.1038/s41598-022-05854-z

Walding N et al (in press) Behaviours of pyroclastic and analogue materials in dry and wet environments for use in experimental modelling of pyroclastic density currents (accepted in Volcanica, 27/09/24)

Walding N, Williams R, Rowley P et al (2023) Cohesional behaviours in pyroclastic material and the implications for deposit architecture. Bull Volcanol 85:67. https://doi.org/10.1007/s00445-023-01682-9

Williams R, Branney MJ, Barry TL (2014) Temporal and spatial evolution of a waxing then waning catastrophic density current revealed by chemical mapping. Geology 42(2):107–110. https://doi.org/10.1130/G34830.1

Wilson CJN (1985) The Taupo eruption, New Zealand. II. The Taupo Ignimbrite. Philos Trans R Soc Lond A Math Phys Sci 314:229–310. https://doi.org/10.1098/rsta.1985.0020

Wilson CJN (1993) Stratigraphy, chronology, styles and dynamics of late Quaternary eruptions from Taupo volcano, New Zealand. Philos Trans R Soc Lond A Phys Eng Sci 343(1668):205–306. https://doi.org/10.1098/rsta.1993.0050

Wright JV, Walker GPL (1981) Eruption, transport and deposition of ignimbrite: a case study from Mexico. J Volcanol Geotherm Res 9(2–3):111–131. https://doi.org/10.1016/0377-0273(81)90001-9

Yang T, Sun H, Cao Y, Luo C, Dodd TJH (2024) Gravel-inlaid mud clasts as indicators of transport processes of subaqueous sediment gravity-flows. Sediment Geol 472:0037–0738. https://doi.org/10.1016/j.sedgeo.2024.106741